


BRIEF REPORT



1-Oxo-3,4-dihydroisoquinoline-4-carboxamides as novel druglike inhibitors of poly(ADP-ribose) polymerase (PARP) with favourable ADME characteristics

Alexander Safrygin^a, Petr Zhmurov^a, Dmitry Dar'in^a, Sergey Silonov^{b*}, Mariia Kasatkina^b, Yulia Zonis^b, Maxim Gureev^c  and Mikhail Krasavin^{a,d}

^aSaint Petersburg State University, Saint Petersburg, Russian Federation; ^bJSC BIOCAD, Saint Petersburg, Russian Federation; ^cDigital Biodesign and Personalized Healthcare Research Center, Sechenov First Moscow State Medical University, Moscow, Russian Federation; ^dImmanuel Kant Baltic Federal University, Kaliningrad, Russian Federation

ABSTRACT

A novel 3,4-dihydroisoquinolin-1-one-4-carboxamide scaffold was designed as the basis for the development of novel inhibitors of poly(ADP-ribose) polymerase (PARP). Synthesis of 3,4-dihydroisoquinolin-1-one-4-carboxylic acids was achieved using the previously developed protocol based on the modified Castagnoli-Cushman reaction of homophthalic anhydrides and 1,3,5-triazinanes as formalimine synthetic equivalents. Employment of 2,4-dimethoxy groups on the nitrogen atom of the latter allowed preparation of 2,3-unsaturated 3,4-dihydroisoquinolinone core building blocks. Iterative synthesis and *in vitro* biological testing of the amides resulting from the amidation of these carboxylic acids allowed not only drawing important structure-activity generalisations (corroborated by *in silico* docking simulation) but also the identification of the lead compound, 4-([1,4'-bipiperidine]-1'-carbonyl)-7-fluoro-3,4-dihydroisoquinolin-1(2*H*)-one, as the candidate for further preclinical development. The lead compound as well as its des-fluoro analog were compared to the approved PARP1 inhibitor, anticancer drug Olaparib, in terms of their molecular characteristics defining druglikeness as well as experimentally determined ADME parameters. The newly developed series demonstrated clear advantages over Olaparib in terms of molecular weight, hydrophilicity, human liver microsomal and plasma stability as well as plasma protein binding. Further preclinical investigation of the lead compound is highly warranted.

ARTICLE HISTORY

Received 6 July 2021
Revised 13 August 2021
Accepted 18 August 2021

KEYWORDS

Poly(ADP-ribose) polymerase; PARP1/2 selectivity; NAD⁺ mimetics; 3,4-dihydroisoquinolinone-4-carboxamides; castagnoli-cushman reaction; druglikeness



1. Introduction

Poly(ADP-ribose) polymerase (PARP) enzymes (numbering seventeen in total) have drawn considerable attention as drug targets in the last decade owing to the clinical success of non-selective PARP1/2 inhibitors *Olaparib*, *Talazoparib*, *Niraparib* and *Rucaparib* approved for cancer treatment¹. PARP1 and PARP2 are two key enzymes that are critical for repairing single-strand breaks ('nicks') in the DNA – a mechanism which is critical for the survival of both normal and cancer cells². During the cell division cycle, single-strand DNA breaks lead to double-strand DNA breaks which can, again, be repaired by the cell's DNA repair machinery, including PARP enzymes. It is generally accepted that, despite the non-selectivity of the approved PARP inhibitors, it is the inhibition of PARP1 that is responsible for the manifestation of their clinical efficacy³. Therefore, attempts have been made towards the development of 'clean', selective PARP1 inhibitors such as compound NMS-P118 developed by Nerviano Medical Sciences jointly with Chemical Diversity Research Institute⁴. The inhibition of PARP1 alone can raise the effectiveness of chemotherapy and radiation therapy⁵. Normal cells do not divide as frequently as cancer cells which allows them to survive PARP1 inhibition. However, tumour


cells with BRCA1, BRCA2 or PALB2 mutations that are synthetically lethal with PARP1 inhibition⁶ are efficiently killed by the drugs of this class.

The pharmacological consequences of PARP2 targeting remain to be unravelled which is somewhat hampered by the scarcity of selective PARP2 inhibitors as pharmacological tools^{7,8}. PARP2 inhibition has been shown to inhibit androgen receptor signalling which may be useful in the prostate cancer therapy⁹.

The majority of PARP1 inhibitors, including those shown in Figure 1, were designed to mimic the nicotinamide moiety of NAD⁺ (from which the adenine ribose unit of poly(ADP-ribose) originates) with which the inhibitors compete for the NAD⁺-binding site of PARP1. This mimicry is achieved *via* the use of either a rotationally constrained primary benzamide (as in *Niraparib* and *NMS-P118*) or a benzamide motif embedded in a ring (as in *Olaparib*, *Talazoparib* and *Rucaparib*). Another characteristic feature noticeable in some of the advanced PARP1 inhibitors is the presence of a fluorine atom (highlighted in blue) in the *meta*-position of the NAD⁺-mimicking benzamide moiety (Figure 1). This 'magic fluorine' has been shown to enhance binding to the target⁴.

CONTACT Mikhail Krasavin  mkrasavin@hotmail.com  Institute of Chemistry, Saint Petersburg State University, 26 Universitetskii Prospekt, Peterhof 198504, Russian Federation.

*Current address: Laboratory of structural dynamics, stability and folding of proteins, Institute of Cytology, Russian Academy of Sciences, St. Petersburg 194064 Russian Federation.

 Supplemental data for this article can be accessed [here](#).

© 2021 The Author(s). Published by Informa UK Limited, trading as Taylor & Francis Group.

This is an Open Access article distributed under the terms of the Creative Commons Attribution License (<http://creativecommons.org/licenses/by/4.0/>), which permits unrestricted use, distribution, and reproduction in any medium, provided the original work is properly cited.

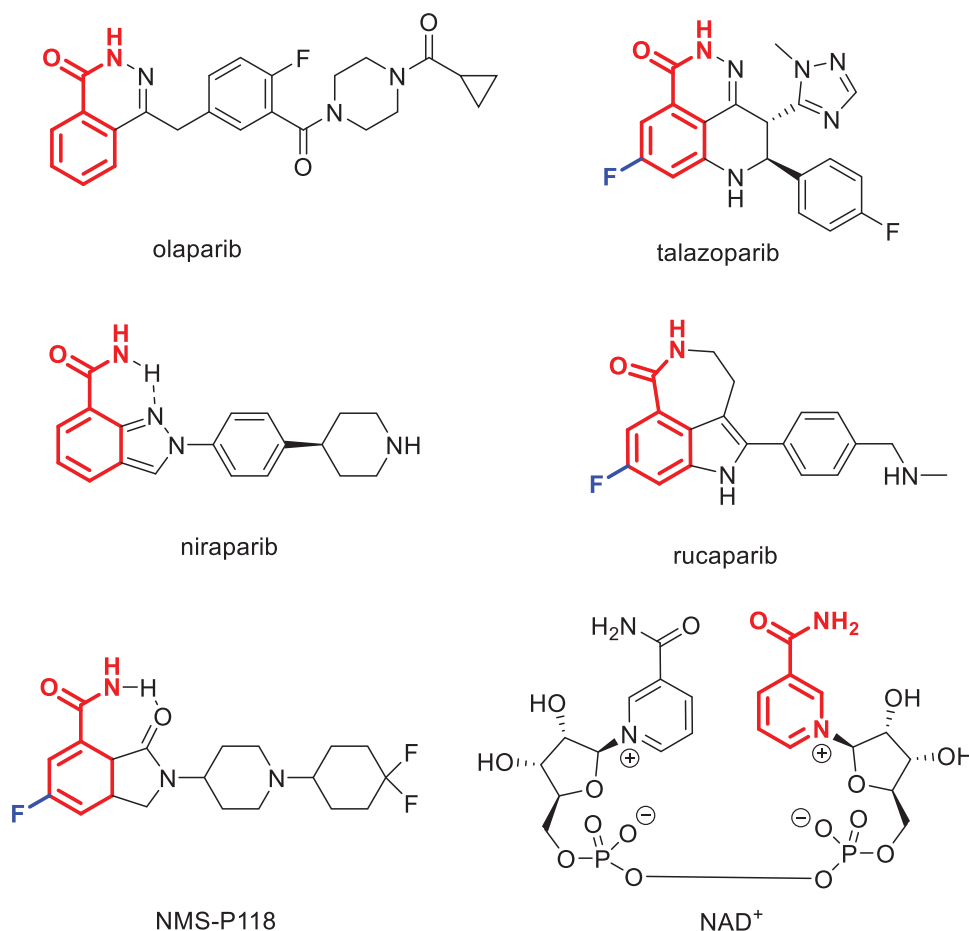


Figure 1. Clinically used PARP1 inhibitors, advanced clinical candidate NMS-P118 (NAD⁺-mimicking motif is highlighted in red, NAD⁺ structure shown).

Analysis of the structures of PARP1 inhibitors shown in Figure 1 as well as those reported in the literature¹⁰ allows one to develop the following intuitive pharmacophore model. The cyclic or conformationally constrained *cis*-benzamide optionally substituted with fluorine in the *meta*-position can be substituted with a periphery substituent in the 'western' portion of the molecule broadly defined either as a combination of a lipophilic linked and a terminal polar hydrogen bond accepting (HBA) or donating (HBD) group or a polar (HBA/HBA) linker capped with a lipophilic terminal moiety. Considering the significant variation in the nature of the 'western' motif in the advanced PARP1 inhibitors, for each new chemotype, the preferred substituent ought to be identified *via* iterative experimental optimisation supported by the computer-aided drug design⁴. Some of the PARP inhibitors reported in the literature do not conform to this general pharmacophore model and, unsurprisingly, are not potent (IC₅₀ in the micromolar range vs. nanomolar values for clinically used PARP1 inhibitors) and display selectivity towards PARP2. For instance, fairly simple benzoate (**1**) and benzamide derivatives of (dihydro)isoquinolone are illustrative examples. Indeed, dihydroisoquinolone **1a** was reported to have PARP1/PARP2 IC₅₀ of 13/0.8 μM and selectivity index (SI) 16.3. Isoquinolone **1b** displayed higher PARP2 selectivity: PARP1/PARP2 IC₅₀ 9.0/0.15 μM (SI 60.0)⁷. Benzamido isoquinolone **2** reported 3 years later displayed a similar profile (PARP1/PARP2 IC₅₀ 13.9/1.5 μM, SI 9.3)⁸. We reasoned that the simple, NAD⁺-mimicking 3,4-dihydroisoquinolone core could be employed in the design of PARP1 inhibitors if the inhibitor molecular topology is adjusted to conform to the general PARP1 inhibitor pharmacophore model (*vide supra*). To this end we set off to explore 1-oxo-

3,4-dihydroisoquinoline-4-carboxamide derivatives **3** – without or with the 'magic fluorine' substitution, respectively (Figure 2). In this Article, we report our findings obtained in the course of realising this idea.

2. Results and discussion

2.1. Chemistry

The synthesis of compounds belonging to series **3** required access to gram quantities of carboxylic acids **4**. Preparation of carboxylic acid **4a** (R¹ = H) had been reported in the patent literature and involved autoclave hydrogenation of isoquinolone-4-carboxylic acid methyl ester, with subsequent hydrolysis¹¹. For this work, we devised a practically convenient method which does not mandate the use of a specialised equipment. The method is reliant on the earlier reported synthesis of 3-unsubstituted isoquinolone-4-carboxylic acid derivatives *via* the Castagnoli-Cushman reaction of 1,3,5-triazinanes as formaldimine synthetic equivalents¹². Reaction of 1,3,5-tris(2,4-dimethoxybenzyl)-1,3,5-triazinane (**5**) with homophthalic (**6a**) or commercially available 7-fluorohomophthalic anhydride (**6b**) furnished carboxylic acids **7a** and **7b**, respectively; the latter were esterified for easier chromatographic purification and the corresponding esters **8a** and **8b** were obtained in 38% and 36% yield over two steps. Removal of the DMB (2,4-dimethoxybenzyl) group by TFA in dichloromethane at room temperature was clean and high-yielding. Esters **9a-b** thus obtained were subjected to basic hydrolysis to furnish the corresponding carboxylic acids **4a-b** in excellent yield (Scheme 1).

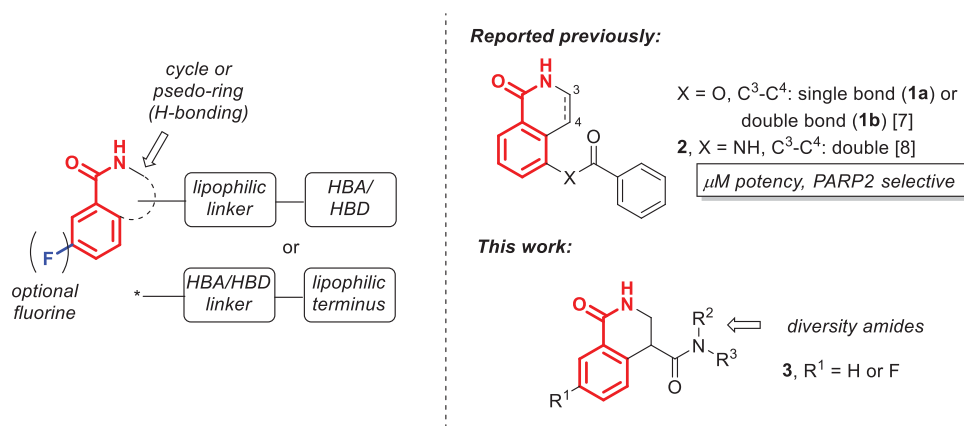
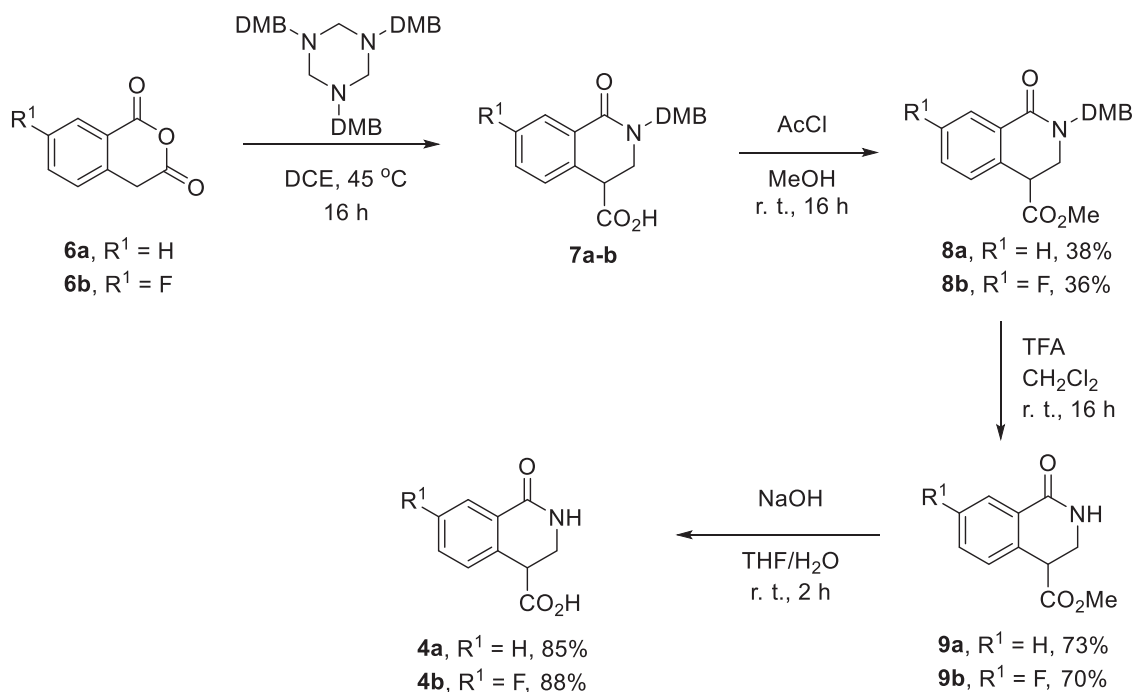


Figure 2. The general PARP1 pharmacophore model; micromolar, PARP2-selective inhibitors 1–2 reported earlier and 1-oxo-3,4-dihydroisoquinoline-4-carboxamides derivatives 3 investigated in this work.



Scheme 1. Synthesis of 1-oxo-3,4-dihydroisoquinoline-4-carboxylic acids **4a-b**.

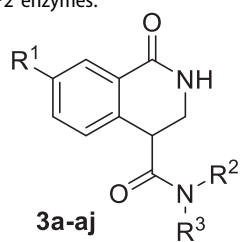
Carboxylic acids **4a-b** were converted to a set of 36 amides **3a-ak** in moderate to good yields (see Table 1 in Section 2.2 for exact chemical yields) using 1-[bis(dimethylamino)methylene]-1*H*-1,2,3-triazolo[4,5-*b*]pyridinium 3-oxide hexafluorophosphate (HATU) as an activating agent for the carboxylic acid function (Scheme 1 and 2). These amides were submitted for the *in vitro* evaluation of their inhibitory potency towards PARP1 and PARP2 enzymes.

2.2. Inhibitory activity against PARP1 and PARP2 *in vitro*

The thirty-six 1-oxo-3,4-dihydroisoquinoline-4-carboxamides **3a-aj** and 1-oxoisoquinoline-4-carboxamide **11** were tested for inhibitory activity towards PARP1 and PARP2 using the commercially available colorimetric activity assay kit from BPS Bioscience (San Diego, CA) in full accordance of the supplier's method description^{13,14}. The initial screening was performed against PARP1 at 1 μ M concentration of each compound, in triplicate ($n=3$) measurements. Compounds which displayed over 80% inhibition

of the enzyme activity were tested in dose-response mode ($n=3$) against PARP1 and PARP2 using Olaparib as the reference inhibitor in order to determine the compounds' half-maximal inhibitory concentration (IC_{50}) and assess the isoform selectivity.

As one can see from the data summarised in Table 1, the unsubstituted ($R^1 = H$) 1-oxo-3,4-dihydroisoquinoline-4-carboxamides **3a-z** displayed fairly 'tight' structure-activity relationships with respect to the amide portion of the molecule. In fact, the majority of the carboxamides did not pass the "80% inhibition at 1 μ M" threshold in order to be progressed to the IC_{50} determination stage. We estimate that these compounds are approximately of the same potency as (3,4-dihydro)isoquinolones **1a-b** and **2** (*vide supra*, Figure 2). However, our goal was to reach into the nanomolar range of half-maximal inhibitory concentrations. To our delight, compound **3i** displayed a markedly potent inhibition of PARP1 (85.2% at 1 μ M) which translated into the IC_{50} of 156 nM vs. PARP1 and about two-fold selectivity towards PARP2 ($IC_{50} = 70.1$ nM). Two striking observations further speak for the

Table 1. Inhibitory activity of compounds **3a-aj** vs. PARP1 and PARP2 enzymes.

Compound	R ¹	R ² NR ³	PARP1		PARP2	SI ^b
			% inhibition at 1 μM	IC ₅₀ , nM ^a (r ²)	IC ₅₀ , nM ^a (r ²)	
3a	H		26.3 ± 7.7	–	–	–
3b	H		42.7 ± 0.9	–	–	–
3c	H		18.6 ± 13.2	–	–	–
3d	H		7.4 ± 8.7	–	–	–
3e	H		56.0 ± 7.5	–	–	–
3f	H		26.2 ± 9.7	–	–	–
3g	H		47.6 ± 4.1	–	–	–
3h	H		27.3 ± 6.0	–	–	–
3i	H		28.9 ± 5.5	–	–	–
3j	H		57.6 ± 5.8	–	–	–
3k	H		45.1 ± 1.7	–	–	–
3l	H		85.2 ± 2.6	156 ± 5.8 (0.9982)	70.1 ± 7.6 (0.9912)	2.23
3m	H		31.2 ± 3.4	–	–	–
3n	H		35.4 ± 5.1	–	–	–

(continued)

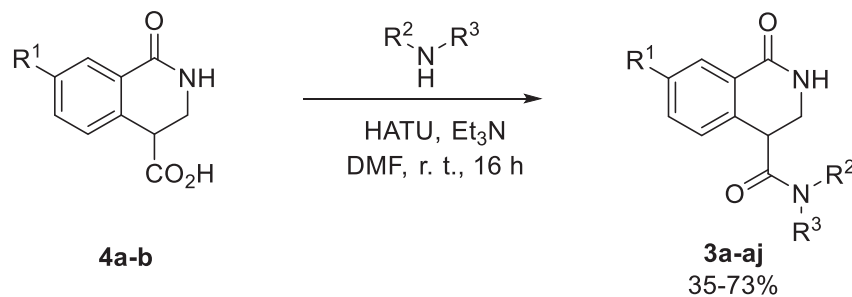
Table 1. Continued.

Compound	R ¹	R ² NR ³	PARP1		PARP2	SI ^b
			% inhibition at 1 μM	IC ₅₀ , nM ^a (r ²)	IC ₅₀ , nM ^a (r ²)	
3o	H		47.4 ± 3.7	–	–	–
3p	H		27.2 ± 4.3	–	–	–
3q	H		32.9 ± 2.4	–	–	–
3r	H		28.5 ± 7.1	–	–	–
3s	H		12.5 ± 8.5	–	–	–
3t ^c	H		43.3 ± 5.9	–	–	–
3u ^c	H		31.9 ± 2.0	–	–	–
3v	H		33.2 ± 4.8	–	–	–
3w ^c	H		66.9 ± 1.5	–	–	–
3x	H		44.6 ± 2.9	–	–	–
3y	H		54.5 ± 4.6	–	–	–
3z	H		45.2 ± 7.4	–	–	–
3aa ^c	F		91.8 ± 0.7	63.1 ± 5.3 (0.9981)	29.4 ± 4.5 (0.9958)	2.17
3ab	F		93.9 ± 0.2	82 ± 6.9 (0.9961)	28.8 ± 4.2 (0.9950)	2.82
3ac	F		95.8 ± 0.7	69.5 ± 8.8 (0.9972)	29.6 ± 6.1 (0.9917)	2.3
3ad	F		92.6 ± 1.1	128 ± 7.1 (0.9957)	40.4 ± 5.8 (0.9985)	3.23

(continued)

Table 1. Continued.

Compound	R ¹	R ² NR ³	PARP1		PARP2	SI ^b
			% inhibition at 1 μM	IC ₅₀ , nM ^a (r ²)	IC ₅₀ , nM ^a (r ²)	
3ae	F		96.6 ± 0.3	55.0 ± 9.9 (0.9894)	20.6 ± 2.5 (0.9998)	2.61
3af	F		96.9 ± 0.5	95.6 ± 11.5 (0.9947)	19.4 ± 3.7 (0.9992)	5.05
3ag	F		95.0 ± 0.9	102 ± 9.4 (0.9956)	22.0 ± 5.6 (0.9805)	4.63
3ah	F		81.9 ± 1.8	371 ± 42 (0.9719)	83.1 ± 6.9 (0.9841)	4.46
3ai	F		93.7 ± 0.8	148 ± 17 (0.9873)	42.0 ± 2.3 (0.9901)	3.52
3aj	F		90.5 ± 0.1	266 ± 25 (0.9833)	44.1 ± 3.9 (0.9989)	6.05
11 ^d	H		49.1 ± 2.6	–	–	–
Olaparib			98.4 ± 2.1	2.8 ± 0.3 (0.9991)	0.7 ± 0.2 (0.9923)	3.98

^aMean (n = 3) ± SD.^bSelectivity index (PARP2 over PARP1).^cIsolated as a trifluoroacetate salt after HPLC.^dSynthesised by amidation of 1-oxisoquinoline-4-carboxylic acid **10**.Scheme 2. Synthesis of 1-oxo-3,4-dihydroisoquinoline-4-carboxamides **3a-aj**.

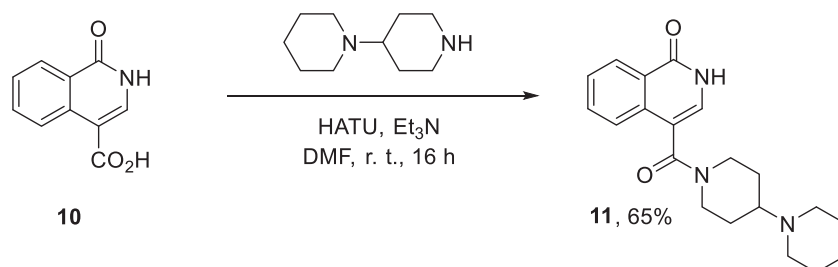
'tightness' of the SAR displayed by this series. Specifically, compounds **3y** (an isostere of **3l**) and **3v** (an oxa-analog of **3l**) are significantly less potent.

Having defined the type of the preferred carboxamide appendage (generally speaking, piperidine bearing a dialkylamino substituent, preferably cyclic, in position 4), we focussed on screening various versions of the appropriately substituted piperidines using the 7-fluoro-substituted core (i.e. *via* the amidation of carboxylic acid **4b**). The effect of the 'magic fluorine' substitution is clearly evident by comparing compounds **3aa** and **3l**. The former displayed a ~2.5-fold better potency compared to the latter although the PARP2/PAPR1 selectivity remained roughly the same.

Modifications of the peripheral cyclic amine did not lead to a significant improvement of the PARP1 potency. Diethylamino compound **3ad** was not significantly different in potency and selectivity from compound **3l**. Ring-contracted and ring-expanded

analogues **3ac** and **3ae**, respectively, displayed similar profiles to that of compound **3aa**. Although compound **3ae** possesses the best activity profile among the compounds investigated in this study, we attribute the marginal improvement of potency compared to compound **3aa** to the lipophilic efficiency (LE)¹⁷ resulting from the introduction of an additional methylene unit. Thus, compound **3aa** can be regarded as the lead structure identified in this study. Although its potency is an order of magnitude lower than that of the clinically used Olaparib, compound **3aa** possesses lower molecular weight and excellent ADME characteristics (*vide infra*) and thus can be considered a frontrunner candidate for further preclinical development.

Interestingly, various substitutions around the distal piperidine ring of **3aa** (i.e. those present compounds **3ab** and **3af-aj**) – although had some negative bearing on the PARP1 potency – did not affect significantly the PARP2 activity. Indeed, compound **3af**



Scheme 3. Synthesis of 1-oxisoquinoline-4-carboxamide **11**.

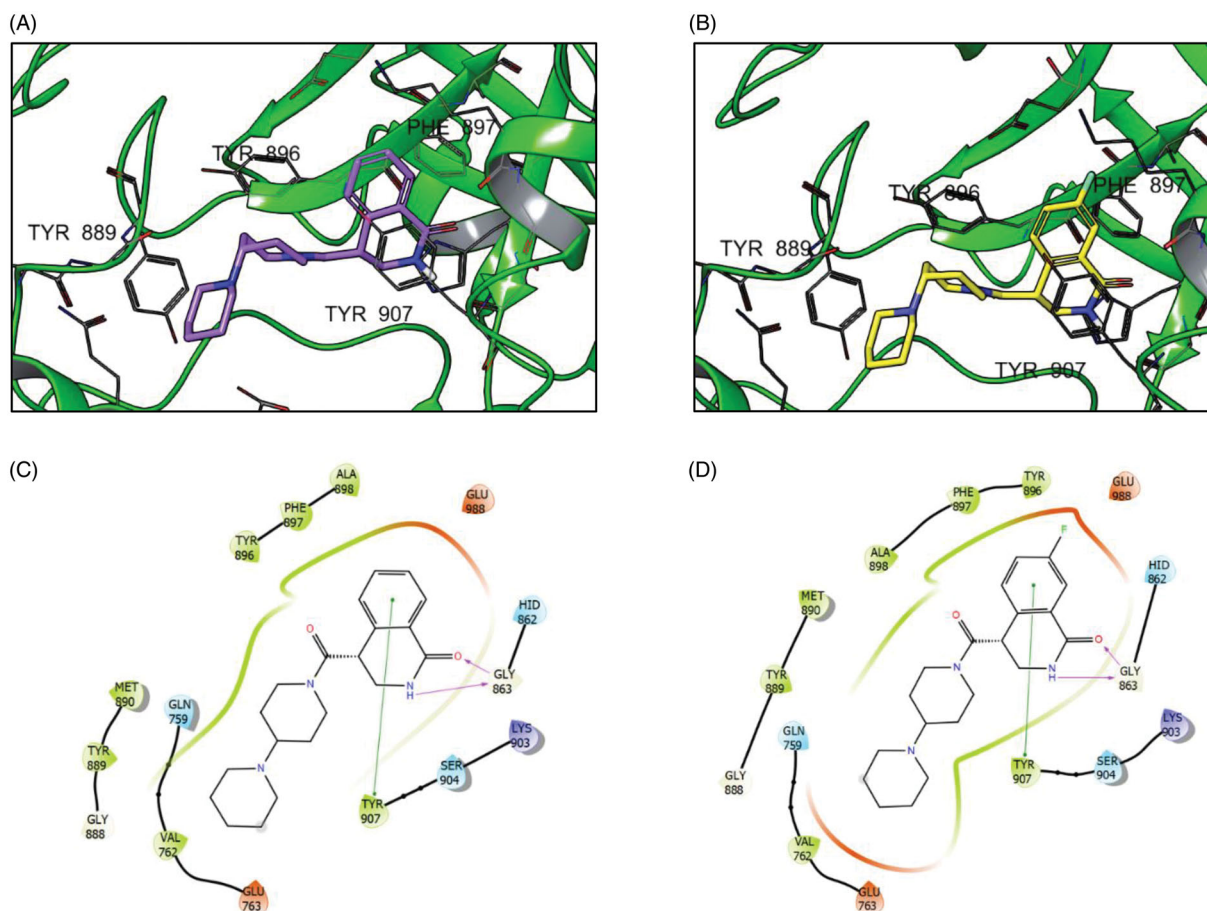


Figure 3. Binding poses of compounds **31** (A) and **3aa** (B) with PARP1 and the respective interaction diagrams (C and D).

can be regarded as the most potent and selective PARP2 inhibitor whose use can be envisioned as a tool compound for further investigation of the fundamental role of PARP2 and its inhibition in various cellular processes. The highest PARP2 selectivity displayed by compound **3aj** is also noteworthy.

It is evident that the flat, isoquinolone scaffold of similar topology is not suitable for a potent PARP inhibitor design. Indeed, compound **11** (the 3,4-dehydro analog of compound **31** or its 7-fluoro version, **3aa**) displayed an approximately 10-fold lower potency.

2.3. Structure-activity relationships rationalised through docking simulation

We attempted to rationalise several notable SAR observations made in the previous section of this Article by performing docking

simulation as well as binding energy calculations for pairwise comparison of certain analogues. These studies were conducted for both enantiomers of each compound and yielded similar results. For brevity, results for only one enantiomer are shown.

2.3.1. Comparison of frontrunner compound **3aa** and its des-fluoro analogue **3i**: the ‘magic fluorine effect’

Docking simulation of both compounds revealed that their docking poses are, not unexpectedly, very similar (Figure 3). However, the important contacts with Tyr896, Ala898 and Phe897 residues are significantly enhanced in the 7-fluoro analogue (**3aa**). Moreover, the contacts with charged Glu988 residue (Coulomb interactions) appear to be enhanced. Analysis of the scoring function components (Table 2) clearly supports these *in silico* observations regarding the ‘magic fluorine’ effect.

2.3.2. Comparison of compounds 3l and 11: the importance of saturated, 3,4-dihydroquinolone scaffold

Aromatisation of the scaffold in compound **11** leading to its increase planarity also induces significant conformational changes in the inhibitors structure and alters its binding to the target. The binding pose of compound **11** in the binding cleft of PARP1 analysed by docking simulation demonstrated the loss of hydrophobic contacts with Met890, Tyr889 and Val762 amino acid residues by compound **11** vs. compound **3l** (Figure 4). This observation is highlighted by the scoring function component analysis showing the loss of the binding affinity to be associated mostly with the hydrophobic and coulombic energy terms (Table 3).

2.3.3. Comparison of compounds 3l and 3v: the detrimental effect of the oxygen atom on potency

In this case, we used MM-GBSA method for the analysis of the binding energy (ΔG) component. The per-atom ΔG value appeared to be the most informative parameter which provided a clear indication of the favorability of the ligand-protein complex formation and took into account the presence of the solvent as

well as the ligand-induced effects on the protein conformation. As can be seen from the total ΔG values as well as per-atom energy components calculated for compounds **3l** and **3v** (Table 4) the morpholine oxygen atom appears to increase the ligand strain. Introduction of the oxygen atom into the distal six-membered ring (**3l** \rightarrow **3v**) induces a conformational rearrangement of the ligand and in the enzyme's binding site, likely due to the changes in the electrostatic profile (Figure 5).

2.3.4. Comparison of compounds 3l and 3y: active vs. inactive isostere

As in the previous case, changing the position of the nitrogen atom in the amide residue (**3l** \rightarrow **3y**, 1,4'-bipiperidine \rightarrow 4-(cyclohexyl)piperazine) alters the configuration on the molecular surface of the ligand and induces the increase in the strain energy and leads to the loss of the ligand-protein affinity. This is clearly demonstrated by the comparison of the per-atom free energy distribution (Table 5) and electrostatic potential isosurfaces (Figure 6) for the two ligands.

Table 2. Docking score values for compounds 3l and 3aa and its components.

Compound	GlideScore (Kcal/mol)	Lipophilic interactions (Kcal/mol)	Coulomb interactions (Kcal/mol)
3aa	-9.91	-3.31	-9.75
3l	-8.57	-2.82	-5.55

Table 3. Docking score values for compounds 3l and 11 and its components.

Compound	GlideScore (Kcal/mol)	Lipophilic interactions (Kcal/mol)	Coulomb interactions (Kcal/mol)
11	-7.76	-2.62	-2.33
3l	-8.57	-2.82	-5.55

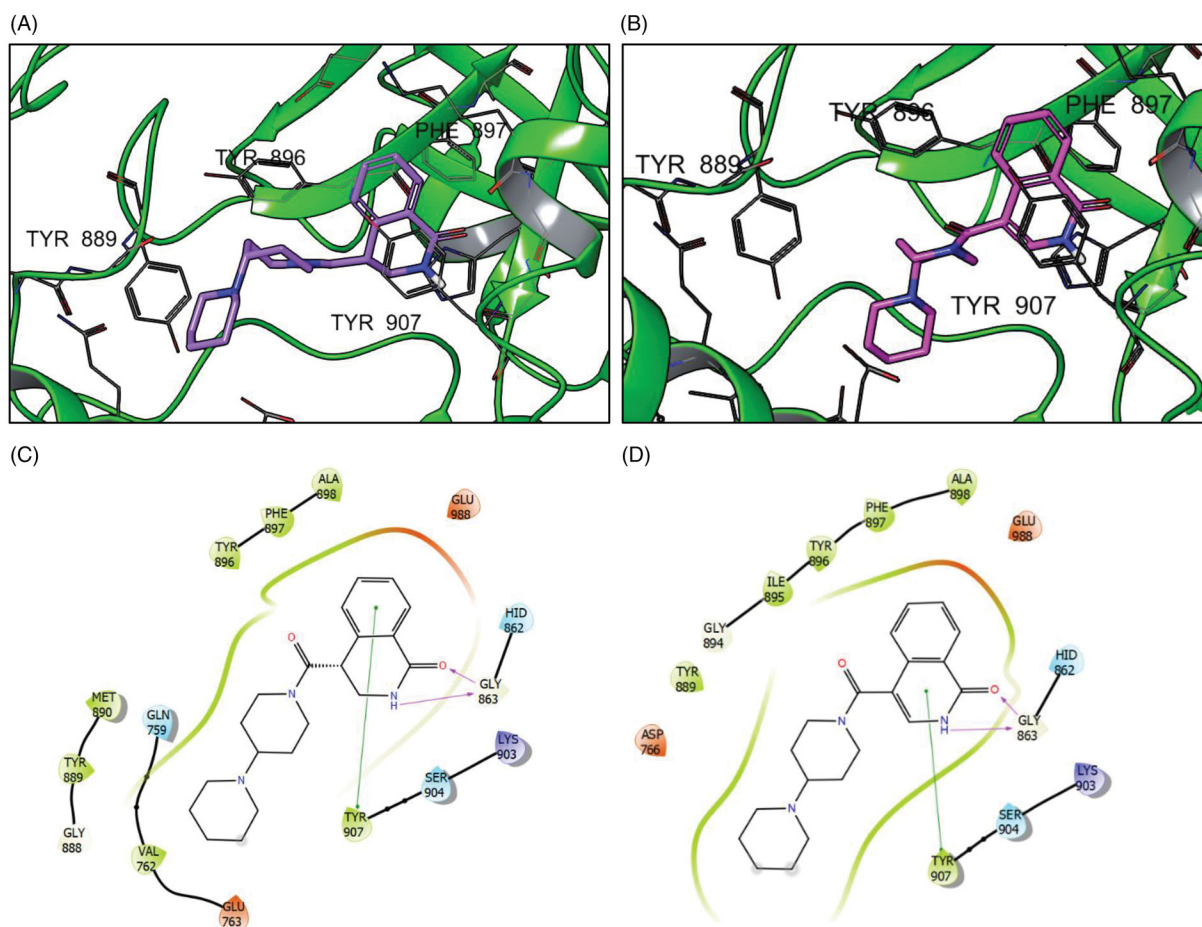


Figure 4. Binding poses of compounds 3l (A) and 11 (B) with PARP1 and the respective interaction diagrams (C and D).

2.4. Druglikeness and ADME parameters

Frontrunner compound **3aa** as well as its non-fluorinated analog **3I** were assayed for aqueous solubility in pH 7.4 phosphate buffer solution, stability in the presence of hepatic S9 fraction, liver microsomes and plasma, as well as for plasma protein binding in comparison with the approved PARP1 inhibitor Olaparib. Additionally, the molecular characteristics such as molecular weight, calculated octanol-water partitioning coefficient (cLogP) as well as hydrogen bond donor (HBD) and acceptor (HBA) count were compared for the two 1-oxo-3,4-dihydroisoquinoline-4-carboxamides and Olaparib (Table 6).

While, of course, the approved PARP1 inhibitor Olaparib is well within the limits of druglikeness as defined by Lipinsky¹⁷ (and so are compounds **3aa** and **3I**), the molecular weight advantage of about 90 Da carried by the 1-oxo-3,4-dihydroisoquinoline-4-carboxamides is evident. Also, the two compounds presented in this work are distinctly more hydrophilic which manifests itself¹⁸ in the markedly lower (by about 20% unbound) plasma protein binding. Quite reassuringly, the frontrunner PARP1 inhibitors developed in this study displayed similar stability in plasma to that of Olaparib. However, their metabolic stability, particularly in the presence of human liver microsomes is significantly higher.

Table 4. Per-atom free energy (ΔG) distribution on PARP1 ligands **3I** and **3v** (red, positive values – unfavourable for binding; green, negative values – favourable for binding).

Binding free energy (ΔG , kcal/mol)	
3I	3v
-47.21	-38.82
6.16	6.04
4.32	4.25
4.53	4.47
0.43	0.36
0.88	0.82
5.73	5.69
0.03	0.09
2.74	2.69
0.37	0.28
0.23	1.82
-1.85	-2.67
-1.32	-1.06
1.21	0.88
-1.06	2.31
3.00	0.01
-1.87	-0.56
0.94	2.99
1.95	3.32
0.31	5.21
1.42	4.28
-2.01	1.69
0.40	3.15
	5.26

3. Conclusion

We have developed a novel series of inhibitors of poly(ADP-ribose) polymerase (PARP) isoforms 1 and 2. Similarly to the marketed PARP1 inhibitor – anticancer drug Olaparib – the best compounds in the series displayed no pronounced selectivity between the two isoforms and some level of selectivity towards PARP2. The analysis of the structure-activity relationships and iterative inhibitors design allowed developing a lead compound whose potency is in the nanomolar range (PARP1/2 IC₅₀ 63.1/29/4 vs. 2.8/0/7 for Olaparib). However, the frontrunner 1-oxo-3,4-dihydroisoquinoline-4-carboxamides are characterised by significantly lower molecular weight and lipophilicity as well as higher metabolic stability and free plasma concentration, compared to Olaparib. These findings clearly warrant further preclinical development of the lead inhibitor, 4-((1,4'-bipiperidine]-1'-carbonyl)-7-fluoro-3,4-dihydroisoquinolin-1(2*H*)-one, as the novel PARP1/2 inhibitor for the treatment of cancer.

4. Experimental section

4.1. General experimental

NMR spectra were recorded on a Bruker Avance III 400 spectrometer (¹H: 400.13 MHz; ¹³C: 100.61 MHz; chemical shifts are reported as parts per million (δ , ppm); the residual solvent peaks were used

Table 5. Per-atom free energy (ΔG) distribution on PARP1 ligands **3I** and **3y** (red, positive values – unfavourable for binding; green, negative values – favourable for binding).

Binding free energy (ΔG , kcal/mol)	
3I	3y
-47.21	-32.01
6.16	6.04
4.32	4.25
4.53	4.47
0.43	0.36
0.88	0.82
5.73	5.69
0.03	0.09
2.74	2.69
0.37	0.28
0.23	1.82
-1.85	-2.67
-1.32	-1.06
1.21	0.88
-1.06	2.31
3.00	0.01
-1.87	-0.56
0.94	2.99
1.95	3.32
0.31	5.21
1.42	4.28
-2.01	1.69
0.40	3.15
	5.26

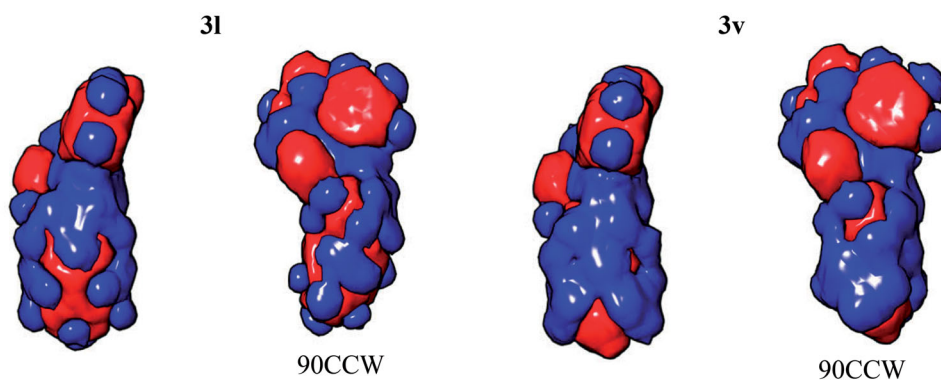


Figure 5. Electrostatic potential isosurfaces for compounds **3I** (active) and **3v** (inactive); 90CCW – view of the ligand rotated 90° counter-clockwise.

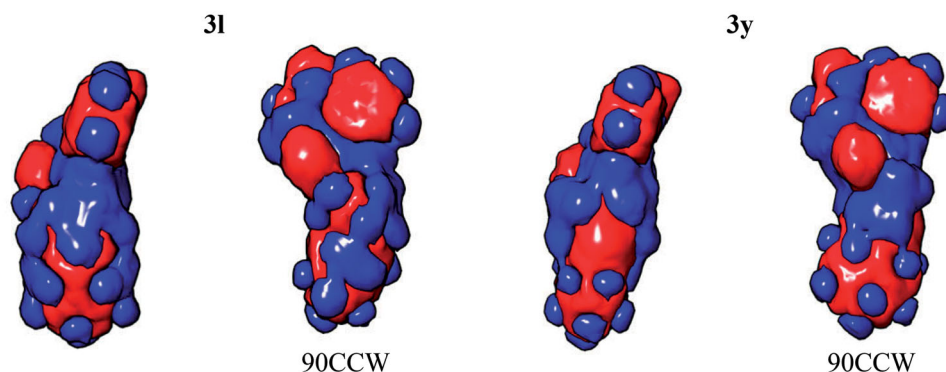


Figure 6. Electrostatic potential isosurfaces for compounds **31** (active) and **3y** (inactive); 90CCW – view of the ligand rotated 90° counter-clockwise.

Table 6. Experimentally determined ADME parameters and calculated molecular characteristics for frontrunner compounds **3aa** and **31** as well as clinically used drug Olaparib.

Compound	Solubility ^a	Stability				Calculated parameters ¹⁶			
		S9 ^b	HLM ^c	Plasma ^d	PPB ^e	MW	cLogP	HBD	HBA
Olaparib	>100	1.1	15	100	90.2	434.5	2.52	1	7
3aa	>100	0.1	3.4	100	71.0	359.4	1.73	1	5
31	>100	0.3	2.6	92.6	66.8	341.5	1.59	1	5

^aSolubility (μM) in pH 7.4 0.01 M phosphate buffer solution; ^bStability in the presence of hepatic S9 fraction ($\mu\text{L}/\text{min}/\text{mg}$); ^cStability in the presence of human liver microsomes ($\mu\text{L}/\text{min}/\text{mg}$); ^d% compound remaining after incubation (4 h) with human plasma; ^eplasma protein binding (% bound).

as internal standards: 7.28 ¹H in CDCl₃, 77.02 ppm for ¹³C in CDCl₃; multiplicities are abbreviated as follows: s=singlet, d=doublet, t=triplet, q=quartette, m=multiplet, br=broad; coupling constants, *J*, are reported in Hz. Mass spectra were recorded on a Bruker microTOF spectrometer (ESI ionization). Melting points were determined in open capillary tubes on Stuart SMP30 Melting Point Apparatus.

4.2. Synthetic organic chemistry

4.2.1. General procedure for the preparation of amides **3a-aj**, **11**

A mixture of corresponding acid (0.50 mmol) and HATU (0.55 mmol, 209 mg) in dry DMF (1 ml) was stirred at room temperature for 15 min. After that amine (0.55 mmol) and triethylamine (0.55 mmol, 56 mg) were added. If amine was in the form of a hydrochloride salt, an additional equivalent of triethylamine was added. The mixture was stirred at room temperature for 16 h. Solvent was evaporated under reduced pressure. Chloroform (6 ml) and saturated sodium bicarbonate solution (3 ml) were added to residue. A mixture was thoroughly shaken, organic layer was separated. Aqueous phase was additionally extracted with chloroform (3 ml). Organic phases were combined, dried over Na₂SO₄ and the solvent was evaporated. The crude amide product was purified by column chromatography on silica gel using ethyl acetate-methanol-triethylamine 25:1:1 as eluent.

4.2.1.1. Ethyl 4-(1-oxo-1,2,3,4-tetrahydroisoquinoline-4-carbonyl)-piperazine-1-carboxylate (3a). Yield 58 mg (35%); Yellow viscous oil; ¹H NMR (400 MHz, DMSO-*d*₆) δ 7.93–7.87 (m, 1H), 7.88 (dd, *J* = 7.7, 1.4 Hz, 1H), 7.49 (td, *J* = 7.5, 1.5 Hz, 1H), 7.40 (td, *J* = 7.5, 0.8 Hz, 1H), 7.15 (d, *J* = 7.5 Hz, 1H), 4.49–4.43 (m, 1H), 4.08 (q, *J* = 7.1 Hz, 2H), 3.68–3.60 (m, 2H), 3.60–3.53 (m, 2H), 3.53–3.42 (m, 5H), 3.42–3.35 (m, 1H), 1.21 (t, *J* = 7.1 Hz, 3H); ¹³C NMR (101 MHz,

DMSO-*d*₆) δ 169.5, 164.5, 155.1, 138.5, 132.2, 130.5, 127.72, 127.66, 126.8, 61.4, 45.5, 44.1, 43.7, 42.7, 41.6, 15.0; HRMS (ESI+), *m/z* calcd for C₁₇H₂₁N₃NaO₄ [M + Na]⁺ 354.1424, found 354.1409.

4.2.1.2. 4-(4-Methylpiperidine-1-carbonyl)-3,4-dihydroisoquinolin-1(2H)-one (3b). Yield 89 mg (65%); Light yellow viscous oil; ¹H NMR (400 MHz, CDCl₃) δ 8.10 (d, *J* = 7.5 Hz, 1H), 7.53–7.44 (m, 1H), 7.44–7.37 (m, 1H), 7.18–7.01 (m, 2H), 4.73 (br.d, *J* = 12.5 Hz, 1H), 4.39–4.31 (m, 1H), 3.99–3.84 (m, 2H), 3.59–3.49 (m, 1H), 3.16 (t, *J* = 12.6 Hz, 1H), 2.83–2.65 (m, 1H), 1.85–1.63 (m, 3H), 1.30–1.11 (m, 2H), 1.07–0.96 (m, 3H); ¹³C NMR (101 MHz, CDCl₃) δ 168.7, 165.9, 137.3, 132.5, 129.3, 128.4, 127.8, 125.2, 46.8, 46.1, 43.1, 34.9, 34.0, 31.3, 30.9, 21.7; HRMS (ESI+), *m/z* calcd for C₁₆H₂₀N₂NaO₂ [M + Na]⁺ 295.1417, found 295.1419.

4.2.1.3. N-Benzyl-N-methyl-1-oxo-1,2,3,4-tetrahydroisoquinoline-4-carboxamide (3c). Yield 84 mg (57%); Beige solid; m. p. = 148–149 °C; ¹H NMR (400 MHz, CDCl₃) mixture of rotamers **A** and **B** 3:2, δ 8.14–8.08 (m, 1H **A**, 1H **B**), 7.57–7.30 (m, 8H **A**, 5H **B**), 7.20 (d, *J* = 7.3 Hz, 2H **B**), 7.11 (d, *J* = 7.5 Hz, 1H **B**), 7.04 (d, *J* = 6.6 Hz, 1H **A**, 1H **B**), 4.86–4.77 (m, 1H **A**, 1H **B**), 4.67 (d, *J* = 14.3 Hz, 1H **A**), 4.54 (d, *J* = 17.1 Hz, 1H **B**), 4.38 (dd, *J* = 11.4, 4.9 Hz, 1H **A**), 4.31 (dd, *J* = 11.0, 4.9 Hz, 1H **B**), 4.04–3.92 (m, 1H **A**, 1H **B**), 3.58 (dt, *J* = 12.2, 4.8 Hz, 1H **A**), 3.48 (dt, *J* = 12.0, 4.8 Hz, 1H **B**), 3.17 (s, 3H), 3.08 (s, 3H); ¹³C NMR (101 MHz, CDCl₃) mixture of rotamers **A** and **B** δ 171.0, 170.5, 166.0, 165.9, 137.2, 137.1, 137.0, 136.1, 132.7, 129.2, 129.1, 128.8, 128.6, 128.5, 128.4, 128.22, 128.13, 128.04, 127.97, 127.92, 127.82, 126.0, 125.2, 125.0, 53.7, 51.3, 43.2, 43.0, 41.4, 35.1, 34.7; HRMS (ESI+), *m/z* calcd for C₁₈H₁₉N₂O₂ [M + H]⁺ 295.1441, found 295.1448.

4.2.1.4. N-(4-Chlorobenzyl)-1-oxo-1,2,3,4-tetrahydroisoquinoline-4-carboxamide (3d). Yield 83 mg (53%); Light yellow viscous oil; ¹H NMR (400 MHz, DMSO-*d*₆) δ 8.51 (t, *J* = 5.9 Hz, 1H), 7.91 (br.s, 1H), 7.88 (dd, *J* = 7.7, 1.3 Hz, 1H), 7.51 (td, *J* = 7.5, 1.5 Hz, 1H), 7.42 (dd, *J* = 7.6, 1.0 Hz, 1H), 7.40–7.37 (m, 2H), 7.31–7.25 (m, 3H), 4.31 (dd, *J* = 5.8, 1.6 Hz, 2H), 3.89 (t, *J* = 5.6 Hz, 1H), 3.67–3.52 (m, 2H); ¹³C NMR (126 MHz, DMSO-*d*₆) δ 171.6, 165.2, 138.4, 137.7, 132.9, 131.9, 129.3, 129.2, 128.7, 128.3, 127.9, 127.7, 44.2, 42.6, 42.2; HRMS (ESI+), *m/z* calcd for C₁₇H₁₅ClN₂NaO₂ [M + Na]⁺ 337.0714, found 337.0715.

4.2.1.5. 4-(1,2,3,4-Tetrahydroisoquinoline-2-carbonyl)-3,4-dihydroisoquinolin-1(2H)-one (3e). Yield 110 mg (72%); Beige solid; m. p. = 222–223 °C; ¹H NMR (400 MHz, DMSO-*d*₆) δ 7.94–7.86 (m, 2H), 7.52–7.36 (m, 2H), 7.25–7.17 (m, 4H), 7.18–7.03 (m, 1H), 4.86 (br.s, 1H), 4.82–4.61 (m, 1H), 4.61–4.52 (m, 1H), 3.96–3.64 (m, 2H),

3.61–3.45 (m, 2H), 3.00–2.81 (m, 2H); ^{13}C NMR (101 MHz, DMSO- d_6) δ 169.8, 164.5, 138.6, 134.9, 133.9, 132.1, 130.6, 129.1, 128.9, 127.7, 127.7, 127.0, 126.9, 126.7, 47.2, 44.5, 43.5, 42.7, 29.6; HRMS (ESI+): m/z calcd for $\text{C}_{19}\text{H}_{19}\text{N}_2\text{O}_2$ [$\text{M} + \text{H}$] $^+$ 307.1441, found 307.1435.

4.2.1.6. 4-(4-ethylpiperazine-1-carbonyl)-3,4-dihydroisoquinolin-1(2H)-one (3f). Yield 88 mg (61%); Dark orange viscous oil; ^1H NMR (400 MHz, CDCl_3) δ 8.11 (dd, $J=7.6$, 1.3 Hz, 1H), 7.50 (td, $J=7.5$, 1.4 Hz, 1H), 7.42 (t, $J=7.5$ Hz, 1H), 7.11 (d, $J=7.6$ Hz, 1H), 6.87 (br.s, 1H), 4.34 (dd, $J=11.2$, 5.0 Hz, 1H), 3.93 (ddd, $J=12.5$, 11.4, 1.1 Hz, 1H), 3.92–3.83 (m, 1H), 3.80–3.71 (m, 1H), 3.66–3.58 (m, 2H), 3.54 (dt, $J=12.5$, 5.0 Hz, 1H), 2.60–2.48 (m, 4H), 2.50 (q, $J=7.2$ Hz, 2H), 1.13 (t, $J=7.2$ Hz, 3H); ^{13}C NMR (101 MHz, CDCl_3) δ 168.8, 165.7, 137.0, 132.5, 129.2, 128.5, 127.9, 125.1, 53.2, 52.5, 52.2, 46.0, 43.0, 42.0, 41.2, 11.9; HRMS (ESI+), m/z calcd for $\text{C}_{16}\text{H}_{22}\text{N}_3\text{O}_2$ [$\text{M} + \text{H}$] $^+$ 288.1707, found 288.1709.

4.2.1.7. Ethyl 1-(1-oxo-1,2,3,4-tetrahydroisoquinoline-4-carbonyl)-piperidine-4-carboxylate (3g). Yield 71 mg (43%); White solid; m. p. = 120–121 °C; ^1H NMR (400 MHz, CDCl_3) δ 8.11 (dd, $J=7.6$, 1.1 Hz, 1H), 7.55–7.46 (m, 1H), 7.42 (t, $J=7.5$ Hz, 1H), 7.15–7.00 (m, 1H), 6.79 (br.s, 1H), 4.64–4.46 (m, 1H), 4.35 (dd, $J=11.2$, 4.9 Hz, 1H), 4.19 (q, $J=6.7$ Hz, 2H), 3.93 (t, $J=11.5$ Hz, 2H), 3.54 (dt, $J=12.0$, 4.6 Hz, 1H), 3.29 (br.q, $J=10.0$ Hz, 1H), 3.04 (br.s, 1H), 2.63 (br.s, 1H), 2.11–1.97 (m, 2H), 1.86–1.67 (m, 2H), 1.29 (t, $J=7.1$ Hz, 3H); ^{13}C NMR (101 MHz, CDCl_3) δ 173.9, 168.7, 165.7, 137.0, 132.5, 129.2, 128.6, 128.0, 125.0, 60.8, 45.6, 45.1, 43.1, 41.3, 40.6, 28.8, 28.1, 14.2; HRMS (ESI+), m/z calcd for $\text{C}_{18}\text{H}_{23}\text{N}_2\text{O}_4$ [$\text{M} + \text{H}$] $^+$ 331.1652, found 331.1656.

4.2.1.8. 4-(4-Methylpiperazine-1-carbonyl)-3,4-dihydroisoquinolin-1(2H)-one (3h). Yield 79 mg (58%); Beige solid; m. p. = 163–164 °C; ^1H NMR (400 MHz, CDCl_3) δ 8.12 (dd, $J=7.6$, 1.2 Hz, 1H), 7.51 (td, $J=7.5$, 1.4 Hz, 1H), 7.43 (t, $J=7.5$ Hz, 1H), 7.12 (d, $J=7.6$ Hz, 1H), 6.64 (br.d, $J=3.7$ Hz, 1H), 4.34 (dd, $J=11.3$, 5.0 Hz, 1H), 3.94 (ddd, $J=12.4$, 11.3, 1.1 Hz, 1H), 3.93–3.70 (m, 2H), 3.61 (br.s, 2H), 3.54 (dt, $J=12.4$, 4.9 Hz, 1H), 2.50 (br.s, 4H), 2.37 (s, 3H); ^{13}C NMR (101 MHz, CDCl_3) δ 168.8, 165.6, 136.9, 132.5, 129.2, 128.6, 128.0, 125.1, 55.4, 54.9, 46.0, 43.1, 41.9, 41.2; HRMS (ESI+), m/z calcd for $\text{C}_{15}\text{H}_{20}\text{N}_3\text{O}_2$ [$\text{M} + \text{H}$] $^+$ 274.1550, found 274.1561.

4.2.1.9. 4-(4-Tosylpiperazine-1-carbonyl)-3,4-dihydroisoquinolin-1(2H)-one (3i). Yield 151 mg (73%); Beige solid; m. p. = 228–229 °C; ^1H NMR (400 MHz, DMSO- d_6) δ 7.86–7.82 (m, 2H), 7.66 (d, $J=8.3$ Hz, 2H), 7.49 (d, $J=8.1$ Hz, 2H), 7.42 (td, $J=7.4$, 1.7 Hz, 1H), 7.38 (td, $J=7.5$, 1.1 Hz, 1H), 7.05 (d, $J=7.3$ Hz, 1H), 4.38 (t, $J=6.2$ Hz, 1H), 3.77–3.63 (m, 3H), 3.44–3.39 (m, 2H), 3.21–3.07 (m, 1H), 3.07–2.97 (m, 2H), 2.97–2.80 (m, 2H), 2.43 (s, 3H); ^{13}C NMR (101 MHz, DMSO- d_6) δ 169.5, 164.5, 144.4, 138.3, 132.6, 132.0, 130.5, 130.5, 128.1, 127.7, 127.6, 126.8, 46.6, 46.3, 43.5, 43.3, 42.7, 42.6, 21.5; HRMS (ESI+), m/z calcd for $\text{C}_{21}\text{H}_{24}\text{N}_3\text{O}_4\text{S}$ [$\text{M} + \text{H}$] $^+$ 414.1482, found 414.1495.

4.2.1.10. 4-(Morpholine-4-carbonyl)-3,4-dihydroisoquinolin-1(2H)-one (3j). Yield 70 mg (54%); Yellow viscous oil; ^1H NMR (400 MHz, CDCl_3) δ 8.13 (d, $J=7.6$ Hz, 1H), 7.53 (t, $J=7.0$ Hz, 1H), 7.45 (t, $J=7.5$ Hz, 1H), 7.13 (d, $J=7.5$ Hz, 1H), 6.70 (br.s, 1H), 4.37–4.27 (m, 1H), 4.00–3.84 (m, 2H), 3.84–3.75 (m, 4H), 3.75–3.66 (m, 1H), 3.66–3.51 (m, 3H); ^{13}C NMR (101 MHz, CDCl_3) δ 169.0, 165.6, 136.8, 132.6, 129.2, 128.7, 128.1, 124.98, 67.0, 66.8, 46.4, 43.0, 42.3, 41.1; HRMS (ESI+), m/z calcd for $\text{C}_{14}\text{H}_{17}\text{N}_2\text{O}_3$ [$\text{M} + \text{H}$] $^+$ 261.1234, found 261.1241.

4.2.1.11. 4-(4-Benzylpiperidine-1-carbonyl)-3,4-dihydroisoquinolin-1(2H)-one (3k). Yield 117 mg (67%); Beige solid; m. p. = 191–192 °C; ^1H NMR (400 MHz, CDCl_3) δ 8.12 (d, $J=7.1$ Hz, 1H), 7.55–7.38 (m, 2H), 7.35–7.29 (m, 2H), 7.27–7.20 (m, 1H), 7.20–7.00 (m, 3H), 6.95 (d, $J=16.7$ Hz, 1H), 4.77 (d, $J=12.5$ Hz, 1H), 4.35 (dd, $J=11.3$, 4.7 Hz, 1H), 4.00–3.84 (m, 2H), 3.59–3.49 (m, 1H), 3.13 (t, $J=12.7$ Hz, 1H), 2.78–2.57 (m, 3H), 1.93–1.73 (m, 3H), 1.38–1.18 (m, 2H); ^{13}C NMR (101 MHz, CDCl_3) δ 168.7, 165.9, 139.7, 137.4, 137.2, 132.5, 129.3, 129.1, 128.5, 128.4, 127.8, 126.2, 125.2, 46.7, 46.1, 43.1, 42.9, 42.8, 42.6, 42.3, 41.4, 41.3, 38.4, 38.0, 32.9, 32.0; HRMS (ESI+), m/z calcd for $\text{C}_{22}\text{H}_{25}\text{N}_2\text{O}_2$ [$\text{M} + \text{H}$] $^+$ 349.1911, found 349.1914.

4.2.1.12. 4-([1,4'-Bipiperidine]-1'-carbonyl)-3,4-dihydroisoquinolin-1(2H)-one (3l). Yield 99 mg (58%); Dark red viscous oil; ^1H NMR (400 MHz, CDCl_3) δ 8.12 (d, $J=7.1$ Hz, 1H), 7.54–7.46 (m, 1H), 7.43 (t, $J=7.4$ Hz, 1H), 7.19–7.00 (m, 1H), 6.42 (br.s, 1H), 4.83 (br.d, $J=10.4$ Hz, 1H), 4.39–4.31 (m, 1H), 4.04–3.88 (m, 2H), 3.53 (dt, $J=12.0$, 4.7 Hz, 1H), 3.19 (t, $J=11.4$ Hz, 1H), 2.82–2.48 (m, 6H), 2.09–1.96 (m, 2H), 1.74–1.63 (m, 4H), 1.59 (qd, $J=11.9$, 3.5 Hz, 2H), 1.53–1.45 (m, 2H); ^{13}C NMR (101 MHz, CDCl_3) δ 168.5, 165.6, 137.0, 132.5, 129.2, 128.6, 127.9, 125.1, 62.6, 62.3, 50.5, 50.3, 45.9, 45.3, 43.2, 41.7, 41.3, 28.9, 25.9, 24.4; HRMS (ESI+), m/z calcd for $\text{C}_{20}\text{H}_{28}\text{N}_3\text{O}_2$ [$\text{M} + \text{H}$] $^+$ 342.2176, found 342.2180.

4.2.1.13. 4-(Pyrrolidine-1-carbonyl)-3,4-dihydroisoquinolin-1(2H)-one (3m). Yield 75 mg (61%); Yellow viscous oil; ^1H NMR (400 MHz, CDCl_3) δ 8.12 (dd, $J=7.6$, 1.2 Hz, 1H), 7.49 (td, $J=7.5$, 1.4 Hz, 1H), 7.42 (t, $J=7.5$ Hz, 1H), 7.05 (d, $J=7.6$ Hz, 1H), 6.62 (br.s, 1H), 4.23 (dd, $J=11.7$, 5.1 Hz, 1H), 3.96 (ddd, $J=12.5$, 11.7, 0.8 Hz, 1H), 3.72–3.62 (m, 2H), 3.62–3.53 (m, 3H), 2.11–1.92 (m, 4H); ^{13}C NMR (101 MHz, CDCl_3) δ 168.9, 165.7, 137.0, 132.6, 129.2, 128.6, 127.8, 125.0, 46.9, 46.0, 43.5, 42.7, 26.2, 24.4; HRMS (ESI+), m/z calcd for $\text{C}_{14}\text{H}_{17}\text{N}_2\text{O}_2$ [$\text{M} + \text{H}$] $^+$ 245.1285, found 245.1291.

4.2.1.14. 4-(Azepane-1-carbonyl)-3,4-dihydroisoquinolin-1(2H)-one (3n). Yield 78 mg (57%); Yellow viscous oil; ^1H NMR (400 MHz, CDCl_3) δ 8.11 (dd, $J=7.6$, 1.1 Hz, 1H), 7.49 (td, $J=7.5$, 1.3 Hz, 1H), 7.41 (t, $J=7.5$ Hz, 1H), 7.09 (d, $J=7.6$ Hz, 1H), 6.93 (d, $J=3.7$ Hz, 1H), 4.33 (dd, $J=11.8$, 5.1 Hz, 1H), 4.02–3.90 (m, 2H), 3.67 (dt, $J=14.6$, 4.9 Hz, 1H), 3.57–3.40 (m, 3H), 1.95–1.53 (m, 8H); ^{13}C NMR (101 MHz, CDCl_3) δ 170.1, 165.9, 137.5, 132.6, 129.2, 128.4, 127.8, 125.2, 48.3, 46.3, 43.3, 41.6, 29.7, 27.7, 27.0, 26.8; HRMS (ESI+), m/z calcd for $\text{C}_{16}\text{H}_{21}\text{N}_2\text{O}_2$ [$\text{M} + \text{H}$] $^+$ 273.1598, found 273.1599.

4.2.1.15. 4-(Thiomorpholine-4-carbonyl)-3,4-dihydroisoquinolin-1(2H)-one (3o). Yield 68 mg (49%); Beige solid; m. p. = 171–172 °C; ^1H NMR (400 MHz, CDCl_3) δ 8.12 (d, $J=7.6$ Hz, 1H), 7.51 (td, $J=7.5$, 1.2 Hz, 1H), 7.44 (t, $J=7.5$ Hz, 1H), 7.08 (d, $J=7.6$ Hz, 1H), 6.93 (br.s, 1H), 4.32 (dd, $J=11.1$, 4.9 Hz, 1H), 4.23 (br.s, 1H), 3.99–3.74 (m, 4H), 3.55 (dt, $J=12.4$, 4.9 Hz, 1H), 2.83–2.60 (m, 4H); ^{13}C NMR (101 MHz, CDCl_3) δ 168.9, 165.7, 136.7, 132.6, 129.3, 128.6, 128.1, 125.0, 48.8, 44.7, 43.1, 41.3, 28.3, 27.7; HRMS (ESI+), m/z calcd for $\text{C}_{14}\text{H}_{17}\text{N}_2\text{O}_2\text{S}$ [$\text{M} + \text{H}$] $^+$ 277.1005, found 277.1003.

4.2.1.16. N-(4-Fluorobenzyl)-1-oxo-1,2,3,4-tetrahydroisoquinoline-4-carboxamide (3p). Yield 67 mg (45%); White solid; m. p. = 188–189 °C; ^1H NMR (400 MHz, DMSO- d_6) δ 8.50 (t, $J=5.7$ Hz, 1H), 7.91 (br.s, 1H), 7.88 (d, $J=7.5$ Hz, 1H), 7.51 (td, $J=7.4$, 1.1 Hz, 1H), 7.41 (t, $J=7.3$ Hz, 1H), 7.34–7.24 (m, 3H), 7.15 (t, $J=8.8$ Hz, 2H),

4.31 (d, $J = 5.7$ Hz, 2H), 3.89 (t, $J = 5.6$ Hz, 1H), 3.67–3.51 (m, 2H); ^{13}C NMR (101 MHz, DMSO- d_6) δ 170.9, 164.3, 161.7 (d, $J = 242.1$ Hz), 138.2, 136.0 (d, $J = 3.0$ Hz), 132.2, 130.0, 129.7 (d, $J = 7.9$ Hz), 127.9, 127.7, 127.6, 115.5 (d, $J = 21.4$ Hz), 44.4, 42.7, 42.1; HRMS (ESI+), m/z calcd for $\text{C}_{17}\text{H}_{16}\text{FN}_2\text{O}_2$ $[\text{M} + \text{H}]^+$ 299.1190, found 299.1183.

4.2.1.17. 4-(4-(2-Methoxyphenyl)piperazine-1-carbonyl)-3,4-dihydroisoquinolin-1(2H)-one (3q). Yield 104 mg (57%); Light yellow solid; m. p. = 155–156 °C; ^1H NMR (400 MHz, CDCl_3) δ 8.14 (dd, $J = 7.6, 0.9$ Hz, 1H), 7.52 (td, $J = 7.5, 1.2$ Hz, 1H), 7.45 (t, $J = 7.5$ Hz, 1H), 7.18 (d, $J = 7.6$ Hz, 1H), 7.13–7.06 (m, 1H), 7.00–6.95 (m, 2H), 6.93 (d, $J = 8.1$ Hz, 1H), 6.51 (d, $J = 4.1$ Hz, 1H), 4.41 (dd, $J = 11.4, 5.0$ Hz, 1H), 4.10–3.94 (m, 3H), 3.91 (s, 3H), 3.78 (br.s, 2H), 3.58 (dt, $J = 12.3, 4.9$ Hz, 1H), 3.21–3.12 (m, 4H); ^{13}C NMR (101 MHz, CDCl_3) δ 168.9, 165.6, 152.3, 140.4, 137.0, 132.6, 129.2, 128.7, 128.0, 125.1, 123.8, 121.1, 118.5, 111.5, 55.5, 51.3, 50.7, 46.4, 43.1, 42.3, 41.3; HRMS (ESI+), m/z calcd for $\text{C}_{21}\text{H}_{24}\text{N}_3\text{O}_3$ $[\text{M} + \text{H}]^+$ 366.1812, found 366.1815.

4.2.1.18. 4-(1-Oxa-9-azaspiro[5.5]undecane-9-carbonyl)-3,4-dihydroisoquinolin-1(2H)-one (3r). Yield 80 mg (49%); Light yellow viscous oil; ^1H NMR (400 MHz, CDCl_3) δ 8.16–8.10 (m, 1H), 7.50 (t, $J = 7.4$ Hz, 1H), 7.43 (t, $J = 7.5$ Hz, 1H), 7.16–7.04 (m, 1H), 6.48–6.36 (m, 1H), 4.49–4.41 (m, 1H), 4.41–4.32 (m, 1H), 3.96 (q, $J = 12.6$ Hz, 1H), 3.75–3.48 (m, 5H), 3.27–3.10 (m, 1H), 2.10 (t, $J = 13.3$ Hz, 1H), 1.99 (d, $J = 13.6$ Hz, 1H), 1.74–1.41 (m, 8H); ^{13}C NMR (101 MHz, CDCl_3) δ 168.5, 165.6, 137.1, 132.4, 129.1, 128.5, 127.9, 125.0, 69.9, 61.1, 43.2, 42.0, 41.4, 37.7, 35.9, 35.8, 35.4, 33.5, 26.0; HRMS (ESI+), m/z calcd for $\text{C}_{19}\text{H}_{24}\text{N}_2\text{NaO}_3$ $[\text{M} + \text{Na}]^+$ 351.1679, found 351.1692.

4.2.1.19. 1-oxo-N-(4-(piperidin-1-yl)benzyl)-1,2,3,4-tetrahydroisoquinoline-4-carboxamide (3s). Yield 100 mg (55%); Beige solid; m. p. = 235–236 °C; ^1H NMR (400 MHz, DMSO- d_6) δ 8.41 (t, $J = 5.6$ Hz, 1H), 7.90 (br.s, 1H), 7.88 (dd, $J = 7.7, 1.0$ Hz, 1H), 7.50 (td, $J = 7.5, 1.3$ Hz, 1H), 7.40 (t, $J = 7.2$ Hz, 1H), 7.25 (d, $J = 7.5$ Hz, 1H), 7.11 (d, $J = 8.6$ Hz, 2H), 6.88 (d, $J = 8.6$ Hz, 2H), 4.22 (d, $J = 5.7$ Hz, 2H), 3.88 (t, $J = 5.8$ Hz, 1H), 3.66–3.48 (m, 2H), 3.13–3.06 (m, 4H), 1.65–1.57 (m, 4H), 1.57–1.49 (m, 2H); ^{13}C NMR (101 MHz, DMSO- d_6) δ 170.67, 164.33, 151.22, 138.39, 132.18, 130.01, 129.40, 128.61, 127.80, 127.62, 127.60, 116.27, 50.26, 44.43, 42.70, 42.39, 25.67, 24.39; HRMS (ESI+), m/z calcd for $\text{C}_{22}\text{H}_{25}\text{N}_3\text{NaO}_2$ $[\text{M} + \text{Na}]^+$ 386.1839, found 386.1829.

4.2.1.20. 4-(4-(4-Fluorobenzyl)piperazine-1-carbonyl)-3,4-dihydroisoquinolin-1(2H)-one (3t). This compound was purified with HPLC using MeCN– H_2O as eluent with addition of $\text{CF}_3\text{CO}_2\text{H}$ and isolated as trifluoroacetate salt. Yield 91 mg (38%); Dark brown viscous oil; ^1H NMR (400 MHz, DMSO- d_6) δ 7.93 (br.s, 1H), 7.89 (dd, $J = 7.6, 1.2$ Hz, 1H), 7.60–7.53 (m, 2H), 7.51 (td, $J = 7.5, 1.1$ Hz, 1H), 7.42 (t, $J = 7.4$ Hz, 1H), 7.34 (t, $J = 8.6$ Hz, 2H), 7.16 (br.s, 1H), 4.49 (t, $J = 6.3$ Hz, 1H), 4.34 (br.s, 4H), 3.49 (br.s, 4H), 3.13 (br.s, 4H); ^{13}C NMR (101 MHz, DMSO- d_6) δ 169.6, 164.5, 163.22 (d, $J = 251.0$ Hz), 138.2, 134.0, 132.2, 130.5, 127.8 (d, $J = 12.4$ Hz), 126.7, 116.3 (d, $J = 21.6$ Hz), 79.7, 58.7, 51.6, 51.0, 42.6; HRMS (ESI+), m/z calcd for $\text{C}_{21}\text{H}_{22}\text{FN}_3\text{NaO}_2$ $[\text{M} + \text{Na}]^+$ 390.1588, found 390.1596.

4.2.1.21. 4-(4-(2-Fluorobenzyl)piperazine-1-carbonyl)-3,4-dihydroisoquinolin-1(2H)-one (3u). This compound was purified with HPLC using MeCN– H_2O as eluent with addition of $\text{CF}_3\text{CO}_2\text{H}$ and isolated as trifluoroacetate salt. Yield 84 mg (35%); Brown viscous oil; ^1H NMR (400 MHz, DMSO- d_6) δ 7.89 (br.s, 2H), 7.62–7.08 (m, 7H), 4.47

(br.s, 1H), 4.25 (br.s, 2H), 3.48 (br.s, 4H), 3.11 (br.s, 4H); ^{13}C NMR (101 MHz, DMSO- d_6) δ 169.5, 164.6, 161.6 (d, $J = 245.3$ Hz), 138.3, 134.5, 133.8, 132.2, 131.0, 130.6, 127.8, 127.7, 126.8, 125.3, 116.2 (d, $J = 21.8$ Hz), 79.8, 53.2, 51.9, 51.5, 42.6; HRMS (ESI+), m/z calcd for $\text{C}_{21}\text{H}_{23}\text{FN}_3\text{O}_2$ $[\text{M} + \text{H}]^+$ 368.1769, found 368.1782.

4.2.1.22. 4-(4-Morpholinopiperidine-1-carbonyl)-3,4-dihydroisoquinolin-1(2H)-one (3v). Yield 93 mg (54%); Light brown viscous oil; ^1H NMR (400 MHz, CDCl_3) δ 8.14 (d, $J = 7.6$ Hz, 1H), 7.51 (br.s, 1H), 7.44 (t, $J = 7.4$ Hz, 1H), 7.10 (m, 1H), 6.07 (br.s, 1H), 4.77 (br.s, 1H), 4.40–4.32 (m, 1H), 3.96 (t, $J = 11.3$ Hz, 2H), 3.77 (br.s, 4H), 3.53 (dt, $J = 12.3, 4.9$ Hz, 1H), 3.29–3.16 (m, 1H), 2.92–2.75 (m, 1H), 2.60 (br.s, 4H), 2.54–2.40 (m, 1H), 2.08–1.95 (m, 2H), 1.57–1.48 (m, 2H); ^{13}C NMR (101 MHz, CDCl_3) δ 168.4, 165.4, 137.0, 132.6, 129.1, 128.7, 128.0, 125.0, 67.1, 61.6, 50.1, 49.9, 45.4, 44.9, 43.2, 41.3, 41.0, 29.7, 28.4; HRMS (ESI+), m/z calcd for $\text{C}_{19}\text{H}_{26}\text{N}_3\text{O}_3$ $[\text{M} + \text{H}]^+$ 344.1969, found 344.1979.

4.2.1.23. 4-(Piperazine-1-carbonyl)-3,4-dihydroisoquinolin-1(2H)-one (3w). This compound was purified with HPLC using MeCN– H_2O as eluent with addition of $\text{CF}_3\text{CO}_2\text{H}$ and isolated as trifluoroacetate salt. Yield 77 mg (41%); Light brown viscous oil; ^1H NMR (400 MHz, DMSO- d_6) δ 7.91 (br.s, 1H), 7.88 (dd, $J = 7.6, 1.1$ Hz, 1H), 7.50 (td, $J = 7.5, 1.3$ Hz, 1H), 7.41 (t, $J = 7.3$ Hz, 1H), 7.18 (d, $J = 7.5$ Hz, 1H), 4.48 (t, $J = 6.3$ Hz, 1H), 4.34 (br.s, 4H), 3.84 (br.s, 2H), 3.75 (br.s, 2H), 3.50 (dd, $J = 6.1, 2.8$ Hz, 1H), 3.26–3.05 (m, 5H); ^{13}C NMR (101 MHz, DMSO- d_6) δ 169.7, 164.5, 138.2, 132.2, 130.5, 127.8, 127.7, 126.8, 43.5, 43.2, 42.9, 42.6; HRMS (ESI+), m/z calcd for $\text{C}_{14}\text{H}_{18}\text{N}_3\text{O}_2$ $[\text{M} + \text{H}]^+$ 260.1394, found 260.1396.

4.2.1.24. 4-(4-Cyclopentylpiperazine-1-carbonyl)-3,4-dihydroisoquinolin-1(2H)-one (3x). Yield 100 mg (61%); White solid; m. p. = 177–178 °C; ^1H NMR (400 MHz, CDCl_3) δ 8.13 (dd, $J = 7.5, 1.1$ Hz, 1H), 7.51 (td, $J = 7.5, 1.3$ Hz, 1H), 7.44 (t, $J = 7.5$ Hz, 1H), 7.13 (d, $J = 7.6$ Hz, 1H), 6.26 (br.s, 1H), 4.35 (dd, $J = 11.4, 5.0$ Hz, 1H), 3.96 (t, $J = 12.0$ Hz, 1H), 3.95–3.69 (m, 2H), 3.62 (br.s, 2H), 3.54 (dt, $J = 12.3, 4.9$ Hz, 1H), 2.68–2.51 (m, 5H), 1.96–1.85 (m, 2H), 1.79–1.68 (m, 2H), 1.66–1.55 (m, 2H), 1.50–1.40 (m, 2H); ^{13}C NMR (101 MHz, CDCl_3) δ 168.6, 165.5, 136.9, 132.5, 129.2, 128.7, 128.0, 125.0, 67.2, 52.7, 52.1, 46.0, 43.1, 42.0, 41.2, 30.4, 24.1; HRMS (ESI+), m/z calcd for $\text{C}_{19}\text{H}_{26}\text{N}_3\text{O}_2$ $[\text{M} + \text{H}]^+$ 328.2020, found 328.2033.

4.2.1.25. 4-(4-Cyclohexylpiperazine-1-carbonyl)-3,4-dihydroisoquinolin-1(2H)-one (3y). Yield 109 mg (64%); Light brown solid; m. p. = 197–198 °C; ^1H NMR (400 MHz, CDCl_3) δ 8.12 (d, $J = 7.5$ Hz, 1H), 7.51 (t, $J = 7.5$ Hz, 1H), 7.43 (t, $J = 7.5$ Hz, 1H), 7.12 (d, $J = 7.6$ Hz, 1H), 6.48 (br.s, 1H), 4.35 (dd, $J = 11.4, 4.9$ Hz, 1H), 3.95 (t, $J = 11.9$ Hz, 1H), 3.89–3.70 (m, 2H), 3.62–3.56 (m, 2H), 3.54 (dt, $J = 12.4, 5.0$ Hz, 1H), 2.66 (m, 4H), 2.39–2.31 (m, 1H), 1.91–1.79 (m, 4H), 1.70–1.62 (m, 1H), 1.31–1.21 (m, 4H), 1.18–1.10 (m, 1H); ^{13}C NMR (101 MHz, CDCl_3) δ 168.7, 165.6, 137.0, 132.5, 129.2, 128.6, 127.9, 125.1, 63.5, 49.6, 48.9, 46.6, 43.1, 42.5, 41.2, 28.9, 26.2, 25.8; HRMS (ESI+), m/z calcd for $\text{C}_{20}\text{H}_{28}\text{N}_3\text{O}_2$ $[\text{M} + \text{H}]^+$ 342.2176, found 342.2178.

4.2.1.26. 4-(4-Cycloheptylpiperazine-1-carbonyl)-3,4-dihydroisoquinolin-1(2H)-one (3z). Yield 105 mg (59%); Light brown solid; m. p. = 207–208 °C; ^1H NMR (400 MHz, CDCl_3) δ 8.13 (dd, $J = 7.6, 1.3$ Hz, 1H), 7.52 (td, $J = 7.5, 1.5$ Hz, 1H), 7.44 (t, $J = 7.5$ Hz, 1H), 7.13 (d, $J = 7.6$ Hz, 1H), 6.17 (d, $J = 4.0$ Hz, 1H), 4.35 (dd, $J = 11.4, 5.0$ Hz, 1H), 3.96 (ddd, $J = 12.4, 11.3, 1.1$ Hz, 1H), 3.88–3.71 (m, 2H), 3.62–3.55 (m, 2H), 3.53 (dt, $J = 12.4, 5.0$ Hz, 1H), 2.70–2.59 (br.s, 5H), 1.91–1.81 (m,

3H), 1.76–1.66 (m, 2H), 1.63–1.40 (m, 7H); ^{13}C NMR (101 MHz, CDCl_3) δ 168.7, 165.5, 137.0, 132.6, 129.1, 128.7, 127.9, 125.1, 65.2, 49.2, 48.4, 46.6, 43.2, 42.5, 41.2, 30.0, 28.0, 25.6; HRMS (ESI+), m/z calcd for $\text{C}_{21}\text{H}_{30}\text{N}_3\text{O}_2$ $[\text{M} + \text{H}]^+$ 356.2333, found 356.2323.

4.2.1.27. 4-([1,4'-Bipiperidine]-1'-carbonyl)-7-fluoro-3,4-dihydroisoquinolin-1(2H)-one (3aa). This compound was purified with HPLC using $\text{MeCN-H}_2\text{O}$ as eluent with addition of $\text{CF}_3\text{CO}_2\text{H}$ and isolated as trifluoroacetate salt. Yield 102 mg (43%); Light yellow viscous oil; ^1H NMR (400 MHz, acetone- d_6) δ 7.66 (d, $J=9.0$ Hz, 1H), 7.44–7.17 (m, 3H), 5.28 (br.s, 4H), 4.78 (br.s, 1H), 4.55 (br.s, 1H), 4.40 (br.s, 1H), 3.75 (br.s, 1H), 3.71–3.56 (m, 4H), 3.37 (br.s, 1H), 3.10 (br.s, 2H), 2.33 (br.s, 2H), 2.00–1.75 (m, 5H); ^{13}C NMR (101 MHz, acetone- d_6) δ 168.6, 163.9, 162.0 (d, $J=244.3$ Hz), 134.4, 132.5, 128.7, 118.6 (d, $J=21.9$ Hz), 113.8 (d, $J=23.0$ Hz), 63.5, 50.0, 49.9, 44.2, 42.8, 42.7, 40.4, 39.7, 27.0, 26.1, 23.0, 21.7; HRMS (ESI+), m/z calcd for $\text{C}_{20}\text{H}_{27}\text{FN}_3\text{O}_2$ $[\text{M} + \text{H}]^+$ 360.2082, found 360.2094.

4.2.1.28. 7-Fluoro-4-(4-methyl-[1,4'-bipiperidine]-1'-carbonyl)-3,4-dihydroisoquinolin-1(2H)-one (3ab). Yield 120 mg (64%); White solid; m. p. = 171–172 °C; ^1H NMR (400 MHz, CDCl_3) δ 7.80 (dd, $J=8.8, 2.4$ Hz, 1H), 7.23–6.98 (m, 2H), 6.80 (d, $J=2.4$ Hz, 1H), 4.78 (d, $J=11.4$ Hz, 1H), 4.36–4.25 (m, 1H), 4.02–3.82 (m, 2H), 3.54 (dt, $J=12.1, 4.6$ Hz, 1H), 3.18 (br.s, 1H), 3.02–2.84 (m, 2H), 2.84–2.40 (m, 2H), 2.23–2.07 (m, 2H), 2.07–1.90 (m, 3H), 1.74–1.61 (m, 2H), 1.61–1.45 (m, 2H), 1.31–1.17 (m, 2H), 0.94 (d, $J=6.1$ Hz, 3H); ^{13}C NMR (101 MHz, CDCl_3) δ 168.4, 164.6, 162.3 (d, $J=247.5$ Hz), 132.9, 131.4 (d, $J=7.5$ Hz), 127.3 (d, $J=7.5$ Hz), 119.4 (d, $J=21.3$ Hz), 115.4 (d, $J=23.4$ Hz), 62.1, 46.2, 45.9, 43.2, 41.9, 40.6, 34.6, 31.0, 21.9; HRMS (ESI+), m/z calcd for $\text{C}_{21}\text{H}_{29}\text{FN}_3\text{O}_2$ $[\text{M} + \text{H}]^+$ 374.2238, found 374.2239.

4.2.1.29. 7-Fluoro-4-(4-(pyrrolidin-1-yl)piperidine-1-carbonyl)-3,4-dihydroisoquinolin-1(2H)-one (3ac). Yield 116 mg (67%); Beige solid; m. p. = 141–142 °C; ^1H NMR (400 MHz, CDCl_3) δ 7.80 (d, $J=7.7$ Hz, 1H), 7.22–7.01 (m, 2H), 6.62 (br.s, 1H), 4.63 (br.s, 1H), 4.30 (br.s, 1H), 3.90 (t, $J=10.9$ Hz, 2H), 3.53 (br.s, 1H), 3.25 (br.s, 1H), 2.89 (br.s, 1H), 2.64 (br.s, 4H), 2.32 (br.s, 1H), 2.04 (br.s, 2H), 1.84 (br.s, 4H), 1.69–1.52 (m, 2H); ^{13}C NMR (101 MHz, CDCl_3) δ 168.3, 164.6, 162.3 (d, $J=248.2$ Hz), 132.9, 127.3, 122.5, 119.5, 115.5, 115.3, 61.4, 51.7, 43.2, 40.6, 32.0, 31.3, 23.2; HRMS (ESI+), m/z calcd for $\text{C}_{19}\text{H}_{25}\text{FN}_3\text{O}_2$ $[\text{M} + \text{H}]^+$ 346.1925, found 346.1923.

4.2.1.30. 4-(4-(Diethylamino)piperidine-1-carbonyl)-7-fluoro-3,4-dihydroisoquinolin-1(2H)-one (3ad). Yield 80 mg (46%); Beige solid; m. p. = 134–135 °C; ^1H NMR (400 MHz, CDCl_3) δ 7.80 (dd, $J=8.9, 2.7$ Hz, 1H), 7.24–6.98 (m, 2H), 6.85 (br.s, 1H), 4.79 (d, $J=12.2$ Hz, 1H), 4.32 (dd, $J=10.3, 4.2$ Hz, 1H), 4.02–3.83 (m, 2H), 3.55 (dt, $J=12.4, 4.8$ Hz, 1H), 3.25–3.13 (m, 1H), 2.90–2.69 (m, 2H), 2.69–2.55 (m, 4H), 2.01–1.86 (m, 2H), 1.60–1.45 (m, 2H), 1.07 (t, $J=7.1$ Hz, 6H); ^{13}C NMR (101 MHz, CDCl_3) δ 168.2, 164.7, 162.3 (d, $J=247.5$ Hz), 132.9, 131.4 (d, $J=7.6$ Hz), 127.3 (d, $J=7.5$ Hz), 119.4 (d, $J=21.2$ Hz), 115.3 (d, $J=23.0$ Hz), 57.9, 46.1, 43.5, 43.3, 43.2, 42.1, 40.6, 29.9, 28.5, 13.6, 13.2; HRMS (ESI+), m/z calcd for $\text{C}_{19}\text{H}_{27}\text{FN}_3\text{O}_2$ $[\text{M} + \text{H}]^+$ 348.2082, found 348.2081.

4.2.1.31. 4-(4-(Azepan-1-yl)piperidine-1-carbonyl)-7-fluoro-3,4-dihydroisoquinolin-1(2H)-one (3ae). Yield 86 mg (46%); White solid; m. p. = 179–180 °C; ^1H NMR (400 MHz, CDCl_3) δ 7.78 (dd, $J=8.8, 2.6$ Hz, 1H), 7.23–6.98 (m, 3H), 4.75 (br.s, 1H), 4.35–4.26 (m, 1H), 4.02–3.80 (m, 2H), 3.55 (dt, $J=12.4, 4.7$ Hz, 1H), 3.23–3.11 (m, 1H), 2.86–2.65 (m, 6H), 2.00–1.88 (m, 2H), 1.70–1.56 (m, 8H), 1.56–1.44

(m, 2H); ^{13}C NMR (101 MHz, CDCl_3) δ 168.3, 164.8, 162.2 (d, $J=247.4$ Hz), 133.0, 131.5 (d, $J=7.3$ Hz), 127.4, 119.3 (d, $J=22.2$ Hz), 115.3 (d, $J=23.2$ Hz), 62.1, 61.2, 51.4, 46.0, 45.5, 43.1, 42.0, 41.8, 40.5, 29.6, 29.1, 28.3, 27.0; HRMS (ESI+), m/z calcd for $\text{C}_{21}\text{H}_{29}\text{FN}_3\text{O}_2$ $[\text{M} + \text{H}]^+$ 374.2238, found 374.2249.

4.2.1.32. 4-(3,3-Dimethyl-[1,4'-bipiperidine]-1'-carbonyl)-7-fluoro-3,4-dihydroisoquinolin-1(2H)-one (3af). Yield 114 mg (59%); Light pink solid; m. p. = 182–183 °C; ^1H NMR (400 MHz, CDCl_3) δ 7.80 (dd, $J=8.8, 2.3$ Hz, 1H), 7.26–6.99 (m, 2H), 6.81–6.67 (m, 1H), 4.68 (br.s, 1H), 4.36–4.27 (m, 1H), 3.99–3.85 (m, 2H), 3.55 (dt, $J=12.4, 4.8$ Hz, 1H), 3.25–3.13 (m, 1H), 2.89–2.76 (m, 1H), 2.62–2.38 (m, 3H), 2.16 (br.s, 2H), 1.96–1.83 (m, 2H), 1.65–1.48 (m, 4H), 1.30–1.20 (m, 2H), 0.95 (s, 6H); ^{13}C NMR (101 MHz, CDCl_3) δ 168.2, 164.6, 162.3 (d, $J=247.5$ Hz), 132.9, 131.4, 127.3, 119.4 (d, $J=21.9$ Hz), 115.5, 61.7, 50.7, 45.8, 45.3, 43.2, 41.8, 40.6, 37.9, 30.8, 29.1, 28.1, 27.3, 23.0; HRMS (ESI+), m/z calcd for $\text{C}_{22}\text{H}_{31}\text{FN}_3\text{O}_2$ $[\text{M} + \text{H}]^+$ 388.2395, found 388.2406.

4.2.1.33. 4-(4,4-Dimethyl-[1,4'-bipiperidine]-1'-carbonyl)-7-fluoro-3,4-dihydroisoquinolin-1(2H)-one (3ag). Yield 78 mg (40%); White solid; m. p. = 200–201 °C; ^1H NMR (400 MHz, CDCl_3) δ 7.80 (dd, $J=8.8, 2.7$ Hz, 1H), 7.23–6.98 (m, 2H), 6.86 (d, $J=2.9$ Hz, 1H), 4.78 (d, $J=10.8$ Hz, 1H), 4.31 (dd, $J=10.7, 4.4$ Hz, 1H), 4.02–3.83 (m, 2H), 3.54 (dt, $J=12.4, 4.8$ Hz, 1H), 3.25–3.13 (m, 1H), 2.84–2.67 (m, 1H), 2.63–2.43 (m, 5H), 2.12–1.93 (m, 2H), 1.55 (qd, $J=12.4, 4.0$ Hz, 2H), 1.44 (br.s, 4H), 0.94 (s, 6H); ^{13}C NMR (101 MHz, CDCl_3) δ 168.3, 164.7, 162.3 (d, $J=247.5$ Hz), 132.9, 131.4 (d, $J=7.4$ Hz), 127.2 (d, $J=7.7$ Hz), 119.4 (d, $J=25.3$ Hz), 115.4 (d, $J=23.2$ Hz), 62.0, 61.8, 46.1, 45.8, 43.2, 41.9, 41.5, 40.6, 38.9, 28.6, 28.2; HRMS (ESI+), m/z calcd for $\text{C}_{22}\text{H}_{31}\text{FN}_3\text{O}_2$ $[\text{M} + \text{H}]^+$ 388.2395, found 388.2390.

4.2.1.34. 4-(4,4-Difluoro-[1,4'-bipiperidine]-1'-carbonyl)-7-fluoro-3,4-dihydroisoquinolin-1(2H)-one (3ah). Yield 99 mg (50%); Light brown viscous oil; ^1H NMR (400 MHz, CDCl_3) δ 7.80 (dd, $J=8.8, 2.4$ Hz, 1H), 7.23–6.99 (m, 2H), 6.89 (br.s, 1H), 4.77 (br.s, 1H), 4.35–4.26 (m, 1H), 4.05–3.81 (m, 2H), 3.56 (dt, $J=12.3, 4.7$ Hz, 1H), 2.84–2.58 (m, 5H), 2.12–1.84 (m, 7H), 1.62–1.45 (m, 2H); ^{13}C NMR (101 MHz, CDCl_3) δ 168.3, 164.7, 162.3 (d, $J=247.5$ Hz), 132.8, 131.4 (d, $J=8.1$ Hz), 127.2 (d, $J=7.5$ Hz), 119.4 (d, $J=22.1$ Hz), 115.4 (d, $J=23.4$ Hz), 61.3, 60.9, 45.9, 45.8, 43.2, 41.8, 40.6, 34.6, 34.4, 34.1, 29.3, 28.3; HRMS (ESI+), m/z calcd for $\text{C}_{20}\text{H}_{25}\text{F}_3\text{N}_3\text{O}_2$ $[\text{M} + \text{H}]^+$ 396.1893, found 396.1883.

4.2.1.35. 7-Fluoro-4-(4-fluoro-[1,4'-bipiperidine]-1'-carbonyl)-3,4-dihydroisoquinolin-1(2H)-one (3ai). Yield 138 mg (73%); Light brown viscous oil; ^1H NMR (400 MHz, CDCl_3) δ 7.76 (dd, $J=8.9, 2.7$ Hz, 1H), 7.26 (br.s, 1H), 7.22–6.97 (m, 2H), 4.82–4.59 (m, 2H), 4.30 (dd, $J=10.4, 4.8$ Hz, 1H), 4.03–3.78 (m, 2H), 3.54 (dt, $J=12.5, 4.7$ Hz, 1H), 3.25–3.11 (m, 1H), 2.83–2.66 (m, 3H), 2.64–2.47 (m, 3H), 2.03–1.82 (m, 6H), 1.53 (qd, $J=12.3, 3.8$ Hz, 2H); ^{13}C NMR (101 MHz, CDCl_3) δ 168.3, 164.8, 162.2 (d, $J=247.5$ Hz), 133.0, 131.5 (d, $J=7.4$ Hz), 127.3 (d, $J=7.5$ Hz), 119.3 (d, $J=21.9$ Hz), 115.2 (d, $J=23.5$ Hz), 88.4 (d, $J=170.2$ Hz), 77.3, 61.8, 61.5, 45.3, 43.1, 41.8, 41.5, 40.5, 31.7 (d, $J=19.3$ Hz), 29.2, 28.1; HRMS (ESI+), m/z calcd for $\text{C}_{20}\text{H}_{26}\text{F}_2\text{N}_3\text{O}_2$ $[\text{M} + \text{H}]^+$ 378.1988, found 378.1999.

4.2.1.36. 7-Fluoro-4-(4-methoxy-[1,4'-bipiperidine]-1'-carbonyl)-3,4-dihydroisoquinolin-1(2H)-one (3aj). Yield 127 mg (65%); Beige solid; m. p. = 186–187 °C; ^1H NMR (400 MHz, CDCl_3) δ 7.79 (dd, $J=8.9, 2.8$ Hz, 1H), 7.23–6.98 (m, 2H), 6.89 (br.s, 1H), 4.76 (d, $J=12.2$ Hz, 1H), 4.30 (dd, $J=10.6, 4.7$ Hz, 1H), 4.02–3.81 (m, 2H),

3.54 (dt, $J = 12.5$, 4.8 Hz, 1H), 3.35 (s, 3H), 3.28–3.12 (m, 2H), 2.89–2.77 (m, 2H), 2.62–2.47 (m, 1H), 2.39–2.30 (m, 2H), 2.05–1.89 (m, 5H), 1.69–1.46 (m, 4H); ^{13}C NMR (101 MHz, CDCl_3) δ 168.4, 164.6, 162.3 (d, $J = 247.6$ Hz), 132.9, 131.4 (d, $J = 7.6$ Hz), 127.2 (d, $J = 7.5$ Hz), 119.4 (d, $J = 22.4$ Hz), 115.3 (d, $J = 23.0$ Hz), 76.2, 61.7, 61.4, 55.5, 46.8, 45.8, 45.3, 43.2, 41.8, 40.6, 31.1, 29.4, 28.1; HRMS (ESI+), m/z calcd for $\text{C}_{21}\text{H}_{29}\text{FN}_3\text{O}_3$ $[\text{M} + \text{H}]^+$ 390.2187, found 390.2189.

4.2.1.37. 4-([1,4'-Bipiperidine]-1'-carbonyl)isoquinolin-1(2H)-one (11).. Yield 110 mg (65%); Pale yellow solid; m. p. = 171–174 °C; ^1H NMR (400 MHz, $\text{DMSO}-d_6$) δ 11.52 (br.s, 1H), 8.25 (d, $J = 7.6$ Hz, 1H), 7.75 (t, $J = 7.5$ Hz, 1H), 7.54 (t, $J = 7.6$ Hz, 1H), 7.50 (br.s, 1H), 7.26 (br.s, 1H), 4.56 (br.s, 1H), 3.63 (br.s, 1H), 3.02–2.74 (m, 2H), 2.48–2.37 (m, 5H), 1.85–1.58 (m, 2H), 1.51–1.41 (m, 5H), 1.40–1.30 (m, 3H); ^{13}C NMR (101 MHz, $\text{DMSO}-d_6$) δ 165.7, 161.7, 135.4, 133.3, 128.4, 127.6, 127.3, 126.2, 124.4, 113.1, 62.0, 50.2, 47.0, 28.2, 26.5, 25.0; HRMS (ESI+), m/z calcd for $\text{C}_{20}\text{H}_{26}\text{N}_3\text{O}_2$ $[\text{M} + \text{H}]^+$ 340.2020, found 340.2020.

4.3. In vitro biological testing

4.3.1. Parp1 and PARP2 inhibition assays

The compounds' inhibitory activity towards PARP1 and PARP1 was assessed using the commercially available colorimetric activity assay kit from BPS Bioscience (San Diego, CA) in full accordance of the supplier's method description^{15,16}

4.3.2. Aqueous PBS solubility determination

The stock solution of the compound tested in DMSO (10 mM) was diluted with 0.01 M sodium phosphate buffer solution (pH 7.4) to the concentration of 100 μM , 80 μM , 60 μM , 50 μM , 40 μM , 30 μM , 20 μM and 10 μM . The serially diluted solutions were transferred into a 96-well plate (Corning 3635, UV Plate) and the plate was incubated at 37 °C for 2 h using BioSan PST-60HL-4 thermo shaker. The plate was read at the wavelength of 620 nm using spectrophotometric microplate reader Sunrise (Tecan, Australia). The optical density values were plotted against compound concentration and approximated by a linear relationship to determine the aqueous solubility.

4.3.3. Microsomal and S9 stability determination

The rate of enzymatic degradation of the compound in *liver microsomes* was determined by incubating a mixture containing 0.5 mg/mL of pooled human liver microsomes (XenoTech, USA, cat. # H2620), 10 μM of compound tested, 2 mM β -nicotinamide adenine dinucleotide (Carbosynth, UK, cat. # NN10871) and 4 mM magnesium chloride in 0.1 M sodium phosphate buffer (pH 7.4) in a solid-state thermostat at 37 °C. The rate of enzymatic degradation of the compound in *human liver S9 fraction* was determined by incubating a reaction mixture containing 0.5 mg/mL of pooled S9 human liver fractions (XenoTech, USA, cat # H0610), 10 μM of compound tested, 2 mM β -nicotinamide adenine dinucleotide (Carbosynth, UK, cat # NN10871) and 4 mM magnesium chloride in 0.1 M sodium phosphate buffer (pH 7.4) in a solid-state thermostat at 37 °C. The reaction was stopped with acetonitrile (100 μL MeCN per 100 μL of the reaction mixture). After stopping the reaction, the samples were centrifuged for 10 min at 10,000 rpm. The supernatant was analysed by chromatography using an Agilent 1260 chromatograph (Agilent, United States). Chromatographic analysis was performed in a gradient elution mode at a flow rate

of 1 ml/min. A graph of the dependence of the logarithm of the area of the peak of the substance on time was built. The dependent coefficient of this straight line corresponded to the elimination constant k , on the basis of which the half-life of the drug ($T_{1/2}$) and intrinsic clearance (Cl_{int}) were calculated.

4.3.6. Plasma stability determination

Determination of stability in human blood plasma was carried out using pooled human blood plasma obtained from ten healthy donors. The candidate stock solution (10 mM in DMSO) was diluted with the pooled blood plasma to a concentration of 10 μM (test solution). The test solution was kept in a solid-state thermostat for 4 h at a temperature of 37 °C. HPLC method using an Agilent 1260 chromatograph (Agilent, USA) was employed to determine the peak area of the compounds in the test samples corresponding to the initial test time (before exposure) and the final test time (after incubation in a solid-state thermostat for 4 h at 37 °C) with preliminary precipitation of protein mass with acetonitrile (300 μL MeCN per 100 μL of the reaction mixture). After stopping the reaction, the samples were centrifuged for 10 min at 10,000 rpm and the supernatant was collected. Chromatographic analysis was performed in a gradient elution mode at a flow rate of 1 ml/min.

4.3.7. Plasma protein binding determination

Determination of binding to human blood plasma proteins was carried out using pooled human blood plasma obtained from ten healthy donors. Determination was performed using Thermo Scientific™ Single-RED dialysis plates. Test solutions of the candidate (10 mM in DMSO) were prepared in blood plasma and in 0.01 M sodium phosphate buffer by dilution in pooled blood plasma to a concentration of 10 μM (test solution 1) and in buffer to a concentration of 10 μM (test solution 2), respectively. The test solutions were transferred to the chambers of the dialysis plate, incubated in an Environmental Shaker – Incubator ES-20/60 (Biosan, Latvia) for 4 h at a temperature of 37 °C at a speed of 130–250 rpm. During the incubation, passive diffusion of the unbound compound occurs, and after 4 h, equilibrium is reached between the chambers with plasma with buffer solution. At the end of the incubation time, samples were taken from the chambers of the plate. HPLC analysis performed using an Agilent 1260 chromatograph (Agilent, USA) allowed determination of the peak area of the compounds in the test samples with preliminary precipitation of proteins with acetonitrile (300 μL of acetonitrile per 100 μL of the reaction mixture). After stopping the reaction, the samples were centrifuged for 10 min at 10,000 rpm and the supernatant was collected.

The concentration of the test compound in the buffer and plasma chambers was calculated using the formula:

$$C = \frac{A_{t=4}}{A_{t=0}} \times 10,$$

where $A_{t=0}$ is the value of the peak area of the candidate's test solution on the chromatogram at the initial moment of time;

$A_{t=4}$ is the value of the peak area of the candidate test solution on the chromatogram after the incubation time;

10 is the initial concentration of the candidate in DMSO (10 mM);

The % unbound compound was calculated using the formula:

$$\%Free = \frac{C_1}{C_2} \times 100,$$

where C_1 is the concentration value in the buffer chamber;

C_2 is the value of the concentration in the plasma chamber.

4.4. In silico studies

4.4.1. Protein structure preparation

PARP1 and 2 protein structures was downloaded from RCSB Protein Data Bank (models ID: 4ZZX, 4ZZY, 4ZZZ, 5A00). All model needed to be preprocessed with Protein Prep Wizard tool (Schrodinger suite 2020–4) in order to fix incorrect bond orders, missing sidechains, crystal water removed from model, restrained minimisation of protein structure with H-bond network refinement¹⁹.

4.4.2. Small molecule preparation

Three-dimensional structure of observed small-molecule compounds was generated with use of OPLS3e forcefield. For better accuracy, forcefield was used in order to achieve missing torsions parameterisation²⁰.

4.4.3. Protein-ligand docking: GridBox

GridBoxes for used protein models of PARP1 and 2 was generated with the use of the reference ligand coordinates present in all observed models. No constraints were used. GridBox size was 16 Å, in accordance with the reference ligands size. For docking grid generation, GlideGrid module (Schrodinger suite 2020–4) was employed.

4.4.4. Protein-ligand docking: docking and results filtering

Docking of all observed compounds in the active pocket of PARP1 and 2 was performed with use of Glide module (Schrodinger suite 2020–4)²¹. Reference ligands was redocked into the active site. Best-fitting poses had RMSD less than 1.5Å to initial ligand structure (from PDB model). For each ligand, up to 20 docking solutions were generated. The best-fitting docking pose was selected in accordance with the reference ligand binding mode. Docking solution quality controlled by Emodel parameters and clustering (RMSD \leq 2.2 Å in cluster).

4.4.5. Protein-ligand MM-GBSA

Protein-ligand complexes binding free energy and its components was calculated with the use of MM-GBSA method²². Calculations were performed in the presence of implicit solvent (water) with residue flexibility cut-off of 6.0 Å.

Acknowledgements

The authors thank the Research Centre for Magnetic Resonance and the Centre for Chemical Analysis and Materials Research of Saint Petersburg State University Research Park for obtaining the analytical data.

Disclosure statement

No potential conflict of interest was reported by the author(s).

Funding

This research was supported by the Russian Foundation for Basic Research [grant 21–53-12001]. Maxim Gureev acknowledges the funding from the Ministry of Science and Higher Education of the Russian Federation [grant 075–15-2020–926]. Dr. Petr Zhmurov is indebted to Saint Petersburg State University for his postdoctoral fellowship.

ORCID

Maxim Gureev  <http://orcid.org/0000-0002-0385-922X>

References

1. Park M-T, Lee S-J. Cell cycle and cancer. *J Biochem Mol Biol* 2003;36:60–5.
2. Gibson BA, Kraus WL. New insights into the molecular and cellular functions of poly(ADP-ribose) and PARPs. *Nat Rev Mol Cell Biol* 2012;13:411–24.
3. Mateo J, Lord CJ, Serra V, et al. A decade of clinical development of PARP inhibitors in perspective. *Ann Oncol* 2019;30:1437–47.
4. Papeo G, Posteri H, Borghi D, et al. Discovery of 2-[1-(4,4-Difluorocyclohexyl)piperidin-4-yl]-6-fluoro-3-oxo-2,3-dihydro-1H-isoindole-4-carboxamide (NMS-P118): a potent, orally available, and highly selective PARP-1 inhibitor for cancer therapy. *J Med Chem* 2015;58:6875–98.
5. Rajman L, Chwalek K, Sinclair DA. Therapeutic potential of NAD-boosting molecules: the in vivo evidence. *Cell Metabol* 2018;27:529–47.
6. Lord CJ, Ashworth A. PARP inhibitors: synthetic lethality in the clinic. *Science* 2017;355:1152–8.
7. Pellicciari R, Camaioni E, Costantino G, et al. On the way to selective PARP-2 inhibitors. Design, synthesis, and preliminary evaluation of a series of isoquinolinone derivatives. *Chem Med Chem* 2008;3:914–23.
8. Sunderland PT, Woon ECY, Dhami A, et al. 5-Benzamidoisoquinolin-1-ones and 5-(ω -Carboxyalkyl)isoquinolin-1-ones as Isoform-selective inhibitors of Poly(ADP-ribose) polymerase 2 (PARP-2). *J Med Chem* 2011;54:2049–59.
9. Gui B, Gui F, Takai T, et al. Selective targeting of PARP-2 inhibits androgen receptor signaling and prostate cancer growth through disruption of FOXA1 function. *Proc Natl Acad Sci USA* 2019;116:14573–82.
10. Velagapudi UK, Patel BA, Shao X, et al. Recent development in the discovery of PARP inhibitors as anticancer agents: a patent update (2016–2020). *Expert Opin Ther Pat* 2021;31:609–23.
11. Frackenpohl J, Zeiss H-J, Heinemann I, Willms L, Müller T, Busch M, Von Koskull-Döering P, Rosinger CH, Dittgen J, Hills MJ. US Patent Application 2014302987. 2014.
12. Guranova N, Dar'in D, Krasavin M. Facile access to 3-unsubstituted tetrahydroisoquinolonic acids via the Castagnoli–Cushman reaction. *Synthesis* 2018;50:2001–8.
13. PARP1. Available from: https://bpsbioscience.com/pub/media/wysiwyg/PARPs/80580_1.pdf
14. PARP2. Available from: https://bpsbioscience.com/pub/media/wysiwyg/PARPs/80581_1.pdf
15. Johnson TW, Gallego RA, Edwards MP. Lipophilic efficiency as an important metric in drug design. *J Med Chem* 2018;61:6401–20.

16. Calculated using Molinspiration Chemoinformatics tool. Available from: <https://www.molinspiration.com/>
17. Lipinski CA, Lombardo F, Dominy BW, Feeney PJ. Experimental and computational approaches to estimate solubility and permeability in drug discovery and development settings. *Adv Drug Deliv Rev* 2001;46:3–26.
18. Lázníček M, Lázníčková A. The effect of lipophilicity on the protein binding and blood cell uptake of some acidic drugs. *J Pharm Biomed Anal* 1995;13:823–8.
19. Sastry GM, Adzhigirey M, Day T, et al. Protein and ligand preparation: parameters, protocols, and influence on virtual screening enrichments. *J Comput Aided Mol Des* 2013;27: 221–34.
20. Roos K, Wu C, Damm W, et al. OPLS3e: extending force field coverage for drug-like small molecules. *J Chem Theory Comput* 2019;15:1863–74.
21. Friesner RA, Murphy RB, Repasky MP, et al. Extra precision glide: docking and scoring incorporating a model of hydrophobic enclosure for protein-ligand complexes. *J Med Chem* 2006;49:6177–96.
22. Genheden S, Ryde U. The MM/PBSA and MM/GBSA methods to estimate ligand-binding affinities. *Exp Opin Drug Discov* 2015;10:449–61.